

NASA TECHNICAL NOTE



NASA TN D-7550

NASA TN D-7550

DEPLOYMENT AND PERFORMANCE
CHARACTERISTICS OF 1.5-METER
SUPERSONIC ATTACHED
INFLATABLE DECELERATORS

*by Herman L. Bobon, James Wayne Sawyer,
and Robert Miserentino*

*Langley Research Center
Hampton, Va. 23665*



NATIONAL AERONAUTICS AND SPACE ADMINISTRATION • WASHINGTON, D. C. • JULY 1974

1. Report No. NASA TN D-7550	2. Government Accession No.	3. Recipient's Catalog No.	
4. Title and Subtitle DEPLOYMENT AND PERFORMANCE CHARACTERISTICS OF 1.5-METER SUPERSONIC ATTACHED INFLATABLE DECELERATORS		5. Report Date July 1974	6. Performing Organization Code
		8. Performing Organization Report No. L-9402	10. Work Unit No. 502-32-01-01
7. Author(s) Herman L. Bohon, James Wayne Sawyer, and Robert Miserentino		11. Contract or Grant No.	
9. Performing Organization Name and Address NASA Langley Research Center Hampton, Va. 23665		13. Type of Report and Period Covered Technical Note	
		14. Sponsoring Agency Code	
12. Sponsoring Agency Name and Address National Aeronautics and Space Administration Washington, D.C. 20546		15. Supplementary Notes	
16. Abstract			
<p>Attached-inflatable-decelerator (AID) canopies fabricated from lightweight Nomex cloth and tapes were deployed in a supersonic stream from the base of a 140° conical aeroshell. Characteristics of the deceleration system were obtained over a wide range of Mach number, dynamic pressure, and pitch angle.</p> <p>All models deployed rapidly by ram air and experienced only mild deployment shock loads. Steady-state drag coefficients as high as 1.3 were obtained in the supersonic stream and were relatively insensitive to Mach number, dynamic pressure, and pitch angle. All models were free of fluttering motion. Results also showed that the AID is aerodynamically more efficient without a burble fence in a supersonic stream.</p> <p>Though measured meridian-tape loads were higher than those predicted by theory, the ram-air deployment rates and steady-state drag coefficients were in good agreement with theory. These results indicate that the AID is a stable, efficient decelerator in a supersonic stream and its performance is readily predictable.</p>			
17. Key Words (Suggested by Author(s)) Attached inflatable decelerator (AID) Supersonic decelerator Inflatable structures Supersonic flow Drag Deployment		18. Distribution Statement Unclassified - Unlimited STAR Category 32	
19. Security Classif. (of this report) Unclassified	20. Security Classif. (of this page) Unclassified	21. No. of Pages 40	22. Price* \$3.25

DEPLOYMENT AND PERFORMANCE CHARACTERISTICS OF 1.5-METER SUPERSONIC ATTACHED INFLATABLE DECELERATORS

By Herman L. Bohon, James Wayne Sawyer, and Robert Miserentino
Langley Research Center

SUMMARY

Attached-inflatable-decelerator (AID) canopies fabricated from lightweight Nomex cloth and tapes were deployed in a supersonic stream from the base of a 140° conical aeroshell. Characteristics of the deceleration system were obtained over a wide range of Mach number, dynamic pressure, and pitch angle.

All models deployed rapidly by ram air and experienced only mild deployment shock loads. Steady-state drag coefficients as high as 1.3 were obtained in the supersonic stream and were relatively insensitive to Mach number, dynamic pressure, and pitch angle. All models were free of fluttering motion. Results also showed that the AID is aerodynamically more efficient without a burble fence in a supersonic stream.

Though measured meridian-tape loads were higher than those predicted by theory, the ram-air deployment rates and steady-state drag coefficients were in good agreement with theory. These results indicate that the AID is a stable, efficient decelerator in a supersonic stream and its performance is readily predictable.

INTRODUCTION

Large supersonic decelerators have many potential applications in areas such as recovery of boosters and space hardware, emergency retrieval of orbital-spacecraft personnel, and the deceleration and landing devices in future planetary atmospheric entry missions. To provide a stable supersonic deceleration system, the Langley Research Center initiated an extensive analytical and experimental program to develop an attached inflatable decelerator (AID). The resulting documentation to date is listed in references 1 to 18. An AID consists of a flexible canopy attached directly to the base of the body to be decelerated. One potential application is shown in figure 1 by the artist's concept of an AID attached to a conical aeroshell. The geometry of the canopy can be tailored to different payload shapes, depending on the application for which it is intended. Although the AID is most suitable for application at supersonic speeds, it has been successfully used for stabilization and deceleration of cylindrical stores by the Army at subsonic speeds (refs. 19 and 20).

In the development of the AID for supersonic application, emphasis has been placed on deceleration of planetary entry vehicles such as that for a Mars mission where the AID is attached to the base of a large, blunt conical shell. In previous investigations, attention has been focused on configurations with C_{DA} ratios of approximately 4.5 (i.e., ratio of C_{DA} – product of drag coefficient and frontal area – with the AID deployed to that of the aeroshell prior to AID deployment). Two such concepts are shown in figures 2(a) and 2(b). In wind-tunnel studies of the model in figure 2(a), canopy deployment was initiated by fluid vaporization (see ref. 8), and the models of figure 2(b) were deployed by mechanical ram air inlets located at the base of the aeroshell (see ref. 11).

In the present paper the results of tunnel tests on AID configurations with a C_{DA} ratio of approximately 2.5 are reported. This C_{DA} ratio was identified in reference 11 as the ratio for which the AID can be used most efficiently as the first stage of a two-stage deceleration system. Such a system would consist of deployment of an AID at about Mach 4 for deceleration to Mach 1.5 when the AID may be detached and used to deploy a large subsonic parachute. The potential gain in payload with such a dual system in a Mars mission is illustrated in reference 11. The geometry of an AID for a typical two-stage system as studied in this paper is shown in figure 2(c) with a burble fence and in figure 2(d) without a fence. The deployed canopy surface area as well as the inflated volume is considerably smaller than those of the earlier models, and the rear attachment is shifted outboard to maintain high drag performance. Models were designed and fabricated under contract (ref. 13) and were tested by NASA at Arnold Engineering Development Center (AEDC) in the 16-ft propulsion wind tunnel (16S). Preliminary test results are reported in reference 17.

SYMBOLS

Values are given both in SI Units and in U.S. Customary Units. The measurements and calculations were made in U.S. Customary Units.

A	frontal area
A_f	flow area (total inlet area or base area of canopy)
C_D	drag coefficient based on frontal area
C_d	discharge coefficient for flow through inlets
C_p	pressure coefficient

F_D	axial force
F_L	meridian tape force
M	free-stream Mach number
m_i	mass inside canopy
p_b	base pressure (see fig. 22)
p_i	internal pressure (see fig. 22)
p_o	local total pressure (see fig. 22)
p_1	pressure upstream of orifice (see eqs. (A1) and (A2) of appendix)
p_2	pressure downstream of orifice (see eqs. (A1) and (A2) of appendix)
q	free-stream dynamic pressure
R	universal gas constant
r	maximum canopy radius (excluding burble fence)
T_i	internal temperature
\bar{T}_i	average internal temperature
T_o	local total temperature
t	time
V	canopy volume
\dot{w}	mass flow rate
x	model radial coordinate (see fig. 3)
y	model axial coordinate (see fig. 3)

α	angle of attack
γ	ratio of specific heats

APPARATUS AND TESTS

Models

The AID models consist of a flexible canopy attached to the base of a rigid 140° conical aeroshell. The canopy is basically a uniform-stress structure whose shape is maintained by a balance of external aerodynamic loads and internal pressurization. The canopy shapes were derived by using the isotenoid analysis described in references 1 and 6. Since numerous canopy shapes are permissible, the shape was obtained by using an optimization procedure described in reference 7 which combines the highest drag areas with the lowest canopy weights. Further, the AID model was sized to provide a ratio of deployed area to aeroshell area to satisfy a Mars-mission requirement set forth in reference 11 (i.e., the AID is deployed at high supersonic speeds and decelerates to Mach 1.5 where a large subsonic parachute is deployed).

The model profile coordinates and the pressure coefficient of the front surface are listed in table I and model details are shown in figures 3 and 4. Two profiles were designed; model I (table I(a)) had a burble fence which extended the frontal diameter 10 percent. Model II (table I(b)) did not have a burble fence. The differences in profile shape are indicated in figure 3. As can be seen, the effect of the burble fence is to elongate the shape and thus have more canopy surface area (and internal volume) to provide the same frontal area. (Note that the coordinates $y = 0$ and $x/r = 1$ corresponds to the point of maximum diameter for each canopy shape.) Maximum diameter of the deployed AID is 1.52 m (60 in.) for model I (including the fence) and 1.39 m (54.6 in.) for model II.

Both canopy shapes were designed to have the same point of attachment to the aeroshell structure. The forward attachment is at the outer periphery of the aeroshell ($x/r = 0.6$) and the rear attachment point is at a value of $x/r = 0.38$. (See table I.) The canopy is secured at the attachment points with ring clamps and a rubber compound was used to seal off the internal volume for inflation purposes.

Prior to deployment of the AID in the supersonic stream, the canopy is contained in its stowage compartment shown in figure 3. Deployment is initiated by releasing four spring-loaded ram-air inlets located at the aeroshell periphery. The spring mechanism is attached to the outer ring clamp as shown in figure 4.

The AID canopy was fabricated from lightweight Nomex cloth tailored into gore patterns. The entire canopy is overlaid by 60 meridional tapes, also of Nomex, which are the primary load-carrying members. Physical properties of the canopy and tape materials are listed in table II. The cloth was calendered and coated with Viton to reduce the permeability to the limits shown in the table.

The aeroshell was fabricated from aluminum alloy and was designed to meet the the wind-tunnel requirements at AEDC. No attempts were made to minimize the weight of the aeroshell or other metal parts. Complete details of model design and fabrication are given in reference 13.

Model designations and pertinent details are listed in table III. Five models were fabricated; two models were rigidly attached to the tunnel sting and three models had pivotal adapters which incorporated a spherical bearing to permit aeroshell freedom of $\pm 20^\circ$ in pitch and yaw. The aeroshell was restrained from rotation to prevent tangling of instrumentation leads. The pivotal adapter had a locking pin which could be engaged during a test to fix rigidly the aeroshell to the sting at zero pitch angle. For further details see reference 13.

All models had eight ram-air inlets. (See fig. 3.) Model IB differed from IA only in the rear inlet size. Model IC was identical to IA, but was rigidly mounted to the sting. Models IIA and IIB differed from each other only in the adapter system. Note that the difference in nominal frontal area of models I and II is due to the burble fence extension. The effect of the fence on the aerodynamic shape is also reflected in the 21-percent increase in internal volume.

Instrumentation

Canopy internal pressure and base pressures were measured with 34.5-kPa (5-psid) differential pressure transducers. Base pressure transducers were located on the sting support where it mates with the six-component balance. (See fig. 3.) Each model also had three strain-gage load cells to measure meridional tape transient and steady-state loads. The load cells, each capable of measuring up to 800 N (180 lbf), were installed on each of three meridional tapes symmetrically located on the front surface at $x/r = 0.70$ (see fig. 5). The method of attaching the load cell to the tape is shown in figure 6. Note the small fold gathered in the meridian tape and fabric to insure that all tape loads are transferred to the load cell.

Model aerodynamic forces were measured with an internally mounted, six-component, strain-gage balance to within ± 44 N (± 10 lbf) for the range of loads measured during the tests. In addition, six motion-picture cameras and two television cameras were used to document and monitor the model behavior.

Output from the six-component balance, load cells, and pressure transducer was continuously recorded by oscillographs to monitor model dynamics, and was digitized and code-punched on paper tape for on-line data reduction.

Test Facility

The models were tested in the 16-ft propulsion wind tunnel (16S) at Arnold Engineering Development Center, a continuous-flow tunnel which can operate over a Mach number range from 1.50 to 4.75. For details of the test facility see reference 17

Test Procedure

A schematic sketch of the model located in the test section is shown in figure 7. A front view of a model on the sting is shown in figure 8. The coil shown around the sting in figure 8 is a hydraulic line to the pivoted adapter locking pin. A rear view of the model is shown in figure 9. The AID canopy is firmly package in its stowage compartment (see fig. 3) and held in place at the rear attachment ring with a cord fed through a series of small loops on the meridian tapes (see fig. 9). The cord is also fed through six pyrotechnic cutters equally spaced around the periphery that are used to release the canopy. The forward inlets are also restrained prior to deployment by a cord fed through two pyrotechnic cutters.

Once the prescribed test conditions are established, steady-state data are obtained on the aeroshell and then the canopy is deployed. The deployment was sequenced so that the pyrotechnic cutters restraining the canopy were energized 0.5 second before those restraining the ram-air inlets.

RESULTS AND DISCUSSION

Data were obtained on five models in the propulsion wind tunnel at AEDC. Test conditions are listed in table IV. All models were deployed at $M = 3$ and $q = 5750$ Pa (120 psf); the rigid-mounted models were deployed at angles of attack of 5° and 10° (models IC and IIB, respectively). After deployment, steady-state data were obtained over a wide range of M , q , and α as indicated in the table. Also listed is the total time each model was in the supersonic stream. At the conclusion of each test, the tunnel was shut down successfully without transient unstart loads causing damage to the model fabric or tapes.

AID Deployment Characteristics

In previous AID tests the canopy restraining cord was cut only at two locations and because of rapid deployment, some tangling of the cords was noted (see ref. 8). In the

present investigation, six pyrotechnic cutters used to release the canopy were activated 0.5 second prior to release of the front inlets and all models deployed uniformly without evidence of cord tangling. The models with pivotal adapter were deployed with the pin released so that the aeroshell was free to pitch $\pm 20^\circ$. Review of the high-speed film indicated the aeroshell was relatively free of pitching motion even during deployment; however, post-test inspection revealed evidence of considerable binding of the spherical bearing. Consequently, data on the aeroshell motion are not considered valid.

Deployment sequence.- Photographs from high-speed film showing the unfurling of the AID canopy during deployment are shown in figure 10(a) for model IIA (with pivotal adapter) and figure 10(b) for model IIB (rigid mount). Both models were deployed at $M = 3.0$ and $q = 5750$ Pa (120 psf) and model IIB was deployed at 10° angle of attack.

Time $t = 0$ corresponds to release of the inlets at the aeroshell periphery. (The packaged canopy was freed of its tie-down cord 0.54 second prior to $t = 0$.) During the initial portion of the deployment the canopies remain in the wake of the aeroshell. At about $t = 0.06$ second the canopies reach their most rearward position and begin outward movement against the airstream. Full inflation occurs in less than 0.3 second.

As can be seen, the deployment process is relatively mild and uniform. Even at 10° angle of attack (fig. 10(b)) the canopy movement during deployment was symmetrical and well behaved. No motion of the aeroshell could be detected in figure 10(a); however, as noted previously, binding of the spherical bearing prevented obtaining reliable angular stability data with the pivotal adapter.

A rear view of the deployment of model IIB is shown by the sequence in figure 11. Again the uniformity of canopy unfurling is apparent.

Ram-air deployment rate.- Canopy internal pressure measured during deployment is shown in figure 12. Figures 12(a), 12(b), and 12(c) are for the model with the burble fence, and figures 12(d) and 12(e) are for the model without the fence. The initial pressure pulse shown by the solid curve occurs after the front inlets are facing the stream and just prior to rearward acceleration of the canopy mass. (See ref. 8.) The high-speed film was used to determine the times during inflation when the rear inlets were in the stream and aiding the inflation. These points are noted in the figures.

Theoretical pressure histories based on inlet-flow analysis presented in the appendix are shown in figure 12 by the dashed curves. The theory accounts for permeability of the rear canopy surface and an experimentally determined discharge coefficient for the cloth inlets. As can be seen, the correlation is good.

The pressure histories are very similar for each model with deployment times less than 0.3 second. Model IB was identical to IA except the rear inlets were smaller (see table III). This caused a small increase in total inflation time; however, the maximum inflation pressure was the same. Model IC was identical to IA but was rigidly mounted and deployed at 5° angle of attack; however, the deployment pressure history is essentially unchanged (see figs. 12(a) and 12(c)). Model II had a smaller interval volume than model I (see table III) and, consequently, inflation time was less than that for model I (see figs. 12(d) and 12(e)). Model IIB was deployed at 10° angle of attack with basically no effect on deployment time.

Deployment force. - The dynamic response of the axial-force component of the strain-gage balance measured during deployment is shown in figure 13. The magnitude of the axial load at $t = 0$ is the drag force on the aeroshell prior to AID deployment. Note that the drag-force trace drops below the level of aeroshell drag during the deployment sequence. This is attributed to vibratory response of the strain-gage balance to the initial impact load and should not affect the magnitude of the peak load.

The first spike in the deployment force curves corresponds in time to the valley in the inflation-pressure curves (see fig. 12). At this point the canopy reaches its maximum rearward position, thus the peak load, and begins unfurling into the stream (see fig. 10). Note that after about 0.2 second the drag force is steady and is near peak value though the internal pressure reached peak value at about 0.3 second. (See fig. 12.) The deployment forces are relatively mild; only those of model II exceeded the steady-state drag values, and the most severe opening loads occur for deployment of 10° angle of attack (fig. 13(e)). A reduction in inlet size of model II could extend the deployment time and reduce the opening dynamic loads.

Meridional-tape dynamic forces. - As noted in an earlier section on instrumentation, each model had a strain-gage load cell installed on each of three meridional tapes (see figs. 5 and 6). The loads recorded by the gages during deployment are shown in figure 14 where the gage force (or tape load) is shown as a function of time. (Note small differences in the force scale in each of the figures.)

Comparison of the meridian-tape forces with the axial forces of figure 13 indicates that the peak opening loads were distributed uniformly over the meridian tapes. More importantly, this peak opening load, when distributed over 120 load points (each of 60 meridian tapes attached to the aeroshell at two points) corresponds to tape loads considerably lower than the steady-state loads. The steady-state values of tape forces will be discussed in a later section.

Steady-State Performance

As indicated in table IV, after deployment of the AID at $M = 3$ and $q = 5750$ Pa (120 psf), the Mach number, dynamic pressure, and angle of attack were varied to obtain AID performance under steady-state conditions. Throughout these tests the AID canopy was extremely stable and free of fluttering motion as observed from high-speed film and oscillograph traces of the axial forces. Photographs of models IA and IIA deployed in the Mach 3 stream are shown in figure 15.

Variation of C_D with dynamic pressure. - The drag coefficient is plotted as a function of dynamic pressure in figure 16 for Mach numbers of 3.0 (model I) and 3.7 (model II). The drag coefficient is based on the total frontal area: 1.82 m^2 (19.63 ft^2) on model I and 1.51 m^2 (16.25 ft^2) on model II (see table III). The difference in frontal area is that attributed to the burble fence on model I.

As can be seen for constant Mach number, the drag coefficients are essentially independent of variation in q over the range shown. This suggests that the canopy shapes remain unchanged, or, that for a constant Mach number, the canopy base pressure, internal pressure, and front surface pressure are linear functions of q .

The solid curves are the calculated values of C_D based on the Newtonian pressure coefficients presented in table I for the front surface and using a constant value over the rear surface given by the expression $C_p = -1/M^2$. The comparison of this value of C_p with the measured base pressure recorded before and after AID deployment is shown in figure 17.

The magnitude of C_D (see fig. 16) is considerably greater for model II than model I (1.32 and 1.17, respectively). Although there is a slight difference in design shape of models I and II (see fig. 3), the values of C_D indicate the influence of the burble fence on the performance in a supersonic stream. Examination of measured axial loads revealed that model I had a 5-percent increase in load over model II; however, the burble fence increased the frontal area of model I by 21 percent. These results indicate that the burble fence is aerodynamically inefficient at supersonic speeds. In addition, the absence of the burble fence simplifies the canopy construction (ref. 13). (It should be recalled that the burble fence is required at subsonic speeds for good stability as it fixes the line of flow separation (refs. 6 and 16).)

Variation of C_D with Mach number. - The AID performance as a function of Mach number is shown in figure 18 for all models at zero angle of attack. Both models I and II show a slight reduction in C_D for Mach numbers higher than 3.0 and, as can be seen, is in good agreement with the theory with the base-pressure correction. The data show good consistency between models of the same type where drag was measured at the same Mach number.

Variation of C_D with angle of attack.- The steady-state drag coefficient at $M = 3$ is plotted as a function of angle of attack in figure 19 for models I and II. The upper curve is the C_D of the 140° conical aeroshell alone measured prior to AID deployment. The drag coefficient is essentially constant over the range of α to 10° and a review of high-speed film indicated that all models were extremely stable.

Meridional-tape loads.- Measured meridional-tape loads are compared with calculated loads in figure 20 for model I and in figure 21 for model II. The measured loads shown by the symbols were obtained during steady-state conditions at $\alpha = 0^\circ$. The locations of the load cells on the models are shown in figure 5. Though the tape loads show consistency as a function of dynamic pressure, there is considerable scatter in magnitude of tape loads at a given value of dynamic pressure. This same degree of scatter was also apparent in a static test program on an AID rear surface in reference 18 and may not be too unreasonable in view of the type of construction and the low magnitude of load. (Note from table II that the tape loads are only about 10 percent of breaking strength.) Much larger values of dynamic pressure may serve to equalize the loads somewhat.

It should also be noted that the model I loads are consistently larger than those of model II. The average value of tape load of model I is about 40 percent greater than the average value of model II. This difference must be attributed to the effect of the burble fence on the distribution of loads between the front and back surfaces.

Figures 20 and 21 show that the calculated tape loads are less than those measured. Although the theory is idealized (see ref. 13), the calculated tape load were expected to be equal to or greater than the measured loads. In reference 18 tape loads imposed by a static-pressure environment measured on an AID canopy rear surface were consistently lower than theory because of the relatively large elongations of the tapes. Increasing the tape stiffness in reference 18 resulted in fair agreement between theory and experiment. In the current program, the tape loads are produced in a supersonic stream on the canopy front surface. Consequently, these results suggest that the tape loads imposed on the AID in a supersonic stream are not consistent with statically imposed loads nor with theory. Improvements in the design theory may be required especially for the application of a small AID in a high-dynamic-pressure environment or a very large AID where tape and fabric loads may be a higher percentage of the allowable loads.

CONCLUDING REMARKS

Five models of an attached inflatable decelerator (AID) designed for operation in a supersonic stream were tested in the 16-ft propulsion wind tunnel (16S) at the Arnold Engineering Development Center to determine deployment and performance character-

istics. The AID canopies were fabricated from lightweight Nomex cloth and tapes and mated to the base of a 140° conical aeroshell. Upon deployment the bluff body was 1.5 m (5 ft) in diameter.

All models were successfully deployed within 0.3 second by using mechanical ram-air inlets. Calculated deployment histories compared well with measured data. Three models were deployed at zero angle of attack, one at 5° , and one at 10° . Shock loads during deployment were mild and always less than the steady-state load at the deployment dynamic pressure, except for the deployment at 10° angle of attack.

Steady-state performance data obtained over a Mach number range from 2.4 to 4.5, dynamic pressure range from 1240 Pa (26 psf) to 5750 Pa (120 psf), and angle of attack to 10° indicated the drag coefficient is relatively insensitive to these parameters. The results show that an AID without a burble fence is more aerodynamically efficient than one with a burble fence in a supersonic stream. Throughout the range of tests all models were extremely stable and free of fluttering motion.

Measured loads in the canopy meridian tapes under steady-state conditions were appreciably higher than those predicted by theory. A comprehensive analysis of this difference was not conducted in the present investigation but more attention would have to be given to the structural design if the AID were to be used for a large-scale application.

Langley Research Center,
National Aeronautics and Space Administration,
Hampton, Va., March 11, 1974.

APPENDIX

INLET FLOW ANALYSIS

Ram-air deployment of an AID can be analyzed by assuming ideal gas relations and isentropic flow equations. Air is assumed to flow into the fabric canopy through inlets and out through the porous fabric on the rear surface of the model (see fig. 22). Two flow regimes exist for flow both into and out of the canopy. For flow with $p_2/p_1 \leq 0.528$ (p_1 is pressure upstream of the inlet and p_2 is downstream pressure), sonic velocity is obtained in the throat of the inlet or in the small holes in the fabric and the flow rate is independent of p_2/p_1 . For $p_2/p_1 > 0.528$, the velocity is less than sonic and is dependent on the p_2/p_1 ratio. The following equations are applicable for the various flow regimes (ref. 21):

For $p_2/p_1 \leq 0.528$,

$$\dot{w} = C_d p_1 A_f \left[\frac{\gamma}{RT_0} \left(\frac{2}{\gamma+1} \right)^{\frac{\gamma+1}{\gamma-1}} \right]^{1/2} \quad (A1)$$

For $p_2/p_1 > 0.528$,

$$\dot{w} = C_d p_1 A_f \left\{ \frac{2\gamma}{(\gamma-1)RT_0} \left[\left(\frac{p_2}{p_1} \right)^{2/\gamma} - \left(\frac{p_2}{p_1} \right)^{\frac{\gamma+1}{\gamma}} \right] \right\}^{1/2} \quad (A2)$$

The net flow rate into the canopy is $\dot{w}_{net} = \dot{w}_{in} - \dot{w}_{out}$ and equations (A1) and (A2) are used to define \dot{w}_{in} and \dot{w}_{out} depending on the pressure ratios p_i/p_0 and p_b/p_i . (See fig. 22.) Since the mass of air inside the canopy is given by

$$m_i = \frac{p_i V}{RT_i}$$

a small change in the mass is $\Delta m_i = \frac{\Delta p_i V}{\bar{T}_i R}$, where \bar{T}_i is the average internal temperature and V and R are assumed constant. The net increase in the mass inside the canopy is given by

$$m_{net} = \dot{w}_{net} t$$

APPENDIX - Concluded

or

$$\Delta m_{\text{net}} = \bar{w}_{\text{net}} \Delta t$$

where \bar{w}_{net} is an average net flow rate. Thus,

$$\Delta t = \frac{\Delta m_{\text{net}}}{\bar{w}_{\text{net}}} = \frac{\Delta p_i V}{T_i R \bar{w}_{\text{net}}} \quad (\text{A3})$$

or in differential form,

$$dt = \frac{dp_i V}{T_i R \dot{w}_{\text{net}}} \quad (\text{A4})$$

where T_i is the instantaneous internal temperature and \dot{w}_{net} is the instantaneous net mass flow rate determined by equations (A1) to (A4).

The values of discharge coefficients C_d used in equations (A1) and (A2) for flow through the inlets were taken to be equal to 70 percent of those published for sharp-edged orifices (ref. 22). These values of C_d were found in reference 11 to be applicable to fabric inlets similar to the ones used in the present tests. Values of C_d used in equations (A1) and (A2) for flow through the porous fabric were obtained from reference 12 by relating measured permeability at the pressure level in question to the standard permeability (i.e., $C_d = Q/N$, where Q is the air permeability of the fabric at 124-Pa (0.5-in. H_2O) pressure differential and N is the correlation factor to account for variable differential pressure). For calculations herein $N = 14.4 \text{ sec/m}$ (0.366 sec/in.). Only the permeability of the rear surface of the canopy was considered since the pressure across that surface is much greater than that across the front surface. Correlations of ram-air inflation time histories of several AID models with theory are shown in the text.

REFERENCES

1. Barton, R. Reed: Development of Attached Inflatable Decelerators for Supersonic Application. NASA CR-66613, 1968.
2. Reichenau, David E. A.: Investigation of an Attached Inflatable Decelerator System for Drag Augmentation of the Voyager Entry Capsule at Supersonic Speeds. AEDC-TR-68-71, U.S. Air Force, Apr. 1968.
3. Baker, D. C.: Investigation of an Inflatable Decelerator Attached to a 120-deg Conical Entry Capsule at Mach Numbers From 2.55 to 4.40. AEDC-TR-68-227, U.S. Air Force, Oct. 1968.
4. Gillis, Clarence L.: Aerodynamic Deceleration System for Space Missions. AIAA Paper No. 68-1081, Oct. 1968.
5. Baker, D. C.: Investigation of an Attached Inflatable Decelerator With Mechanically Deployed Inlets at Mach Numbers From 2.25 to 4.75. AEDC-TR-69-132, U.S. Air Force, June 1969.
6. Mikulas, Martin M., Jr.; and Bohon, Herman L.: Development Status of Attached Inflatable Decelerators. J. Spacecraft & Rockets, vol. 6, no. 6, June 1969, pp. 654-660.
7. Anderson, Melvin S.; Bohon, Herman L.; and Mikulas, Martin M., Jr.: A Structural Merit Function for Aerodynamic Decelerators. NASA TN D-5535, 1969.
8. Bohon, Herman L.; and Miserentino, R.: Deployment and Performance Characteristics of 5-Foot-Diameter (1.5 m) Attached Inflatable Decelerators From Mach Number 2.2 to 4.4. NASA TN D-5840, 1970.
9. Deveikis, William D.; and Sawyer, James Wayne: Static Aerodynamic Characteristics, Pressure Distributions, and Ram-Air Inflation of Attached Inflatable Decelerator Models at Mach 3.0. NASA TN D-5816, 1970.
10. Faurote, G. L.; and Burgess, J. L.: Thermal and Stress Analysis of an Attached Inflatable Decelerator (AID) Deployed in the Mars and Earth Atmospheres. NASA CR-111920, 1971.
11. Bohon, Herman L.; and Miserentino, Robert: Attached Inflatable Decelerator (AID) Performance Evaluation and Mission-Application Study. J. Spacecraft & Rockets, vol. 8, no. 9, Sept. 1971, pp. 952-957.
12. Deaton, Jerry W.; and Willis, Conrad M.: The Effects of Uniaxial and Biaxial Tensile Loads and Load Cycling on the Air Permeability of a Lightweight Coated Fabric. AIAA Paper No. 70-1178, Sept. 1970.

13. Johnson, B. A.: Design, Fabrication and Static Testing of First-Stage Attached Inflatable Decelerator (AID) Models. NASA CR-111934, 1971.
14. Creel, Theodore R., Jr.; and Miserentino, Robert: Aerodynamic Heating at Mach 8 of Attached Inflatable Decelerator Configurations. NASA TM X-2355, 1971.
15. Deveikis, William D.; and Sawyer, James Wayne: Flow Patterns and Pressure Distributions Around a Bluff Afterbody in the Wake of a 120° Cone for Various Separation Distances at Mach 3.0. NASA TN D-6281, 1971.
16. Sawyer, James Wayne; and Whitcomb, Charles F.: Subsonic and Transonic Pressure Distributions Around a Bluff Afterbody in the Wake of a 120° Cone for Various Separation Distances. NASA TN D-6569, 1971.
17. Reichenau, David E. A.: Deployment and Performance Characteristics of Attached Inflatable Decelerators With Mechanically Deployed Inlets at Mach Numbers From 2.6 to 4.5. AEDC TR-72-90, U.S. Air Force, June 1972. (Available from DDC as AD 743 303.)
18. Willis, Conrad M.; and Mikulas, Martin M., Jr.: Static Structural Tests of a 1.5-Meter-Diameter Fabric Attached Inflatable Decelerator. NASA TN D-6929, 1972.
19. Flatau, Abraham; Olson, Donald N.; and Miller, Miles C.: The Use of an Attached Inflatable Decelerator for Store Delivery From High Speed Aircraft From Low Altitude. AIAA Paper No. 70-1199, Sept. 1970.
20. Sawyer, James Wayne: Subsonic Pressure Distributions Around a Solid Model of an Inflatable Decelerator Attached to the Base of an Ogive-Cylinder. NASA TM X-2535, 1972.
21. Albertson, Maurice L.; Barton, James R.; and Simons, Daryl B.: Fluid Mechanics for Engineers. Prentice-Hall, Inc., c.1960, p. 561.
22. Shapiro, Ascher H.: The Dynamics and Thermodynamics of Compressible Fluid Flow. Vol. I. Ronald Press Co., c.1953, p. 647.

TABLE I.- AID MODEL PROFILE COORDINATES

(a) Model I

x/r	y/r Front surface	y/r Rear surface	C _p Front surface
1.00000000E+00	0.	0.	7.61904762E-01
9.99000000E-01	3.32819083E-02	-2.18055561E-02	7.03492063E-01
9.75000000E-01	1.57445013E-01	-1.06822237E-01	4.56269841E-01
9.50000000E-01	2.15344557E-01	-1.46923795E-01	4.45268620E-01
9.25000000E-01	2.57259133E-01	-1.74868922E-01	5.17396313E-01
9.00000000E-01	2.91124148E-01	-1.95961495E-01	6.09216590E-01
8.75000000E-01	3.19948723E-01	-2.12278774E-01	7.00329164E-01
8.50000000E-01	3.45388508E-01	-2.24885511E-01	9.10799554E-01
8.25000000E-01	3.55328597E-01	-2.34409186E-01	9.87011839E-01
8.00000000E-01	3.69548927E-01	-2.41240012E-01	1.05166728E+00
7.75000000E-01	4.09314684E-01	-2.45535116E-01	1.10697688E+00
7.50000000E-01	4.27876412E-01	-2.47760148E-01	1.15463943E+00
7.25000000E-01	4.45423735E-01	-2.47712996E-01	1.19597793E+00
7.00000000E-01	4.62103963E-01	-2.45550488E-01	1.23203521E+00
6.75000000E-01	4.78934542E-01	-2.41275627E-01	1.26364227E+00
6.50000000E-01	4.93311462E-01	-2.34552759E-01	1.29146787E+00
6.25000000E-01	5.08013585E-01	-2.26202029E-01	1.31605500E+00
6.00000000E-01	5.22207965E-01	-2.15192459E-01	1.33784809E+00
5.75000000E-01	Forward attachment	-2.01628729E-01	
5.50000000E-01		-1.85228031E-01	
5.25000000E-01		-1.55579370E-01	
5.00000000E-01		-1.42065396E-01	
4.75000000E-01		-1.13725751E-01	
4.50000000E-01		-7.88773238E-02	
4.25000000E-01		-3.41413527E-02	
4.00000000E-01		-2.99577046E-02	
3.80000000E-01		3.00000000E-01	
		Rear attachment	

TABLE I.- AID MODEL PROFILE COORDINATES - Concluded

(b) Model II

x/r	y/r Front surface	y/r Rear surface	C _p Front surface
1.00000000E+00	0.	0.	5.09921654E-29
9.99000000E-01	2.18208275E-02	-2.18055561E-02	1.46988528E-02
9.75000000E-01	1.08690517E-01	-1.08322257E-01	3.16340283E-01
9.50000000E-01	1.52395361E-01	-1.46923759E-01	5.52400894E-01
9.25000000E-01	1.86225965E-01	-1.74868922E-01	7.33439707E-01
9.00000000E-01	2.12351377E-01	-1.95961495E-01	8.75440983E-01
8.75000000E-01	2.35798587E-01	-2.12278774E-01	9.88949159E-01
8.50000000E-01	2.56617725E-01	-2.24885511E-01	1.08115309E+00
8.25000000E-01	2.75437917E-01	-2.34409188E-01	1.15709360E+00
8.00000000E-01	2.92672967E-01	-2.41240072E-01	1.22039212E+00
7.75000000E-01	3.88612555E-01	-2.45535116E-01	1.27370597E+00
7.50000000E-01	3.23459744E-01	-2.47750148E-01	1.31902164E+00
7.25000000E-01	3.37406088E-01	-2.47712998E-01	1.35784882E+00
7.00000000E-01	3.50548378E-01	-2.45550498E-01	1.39135177E+00
6.75000000E-01	3.62998515E-01	-2.41275627E-01	1.42044028E+00
6.50000000E-01	3.74839562E-01	-2.34852759E-01	1.44583370E+00
6.25000000E-01	3.88101055E-01	-2.26202029E-01	1.46810692E+00
6.00000000E-01	3.96961188E-01	-2.15192459E-01	1.48772382E+00
5.75000000E-01	Forward attachment	-2.01528729E-01	
5.50000000E-01		-1.85228031E-01	
5.25000000E-01		-1.55579374E-01	
5.00000000E-01		-1.42068396E-01	
4.75000000E-01		-1.13725751E-01	
4.50000000E-01		-7.88773238E-01	
4.25000000E-01		-3.41413527E-01	
4.00000000E-01		2.99577046E-02	
3.80000000E-01		1.75000000E-01	
		Rear attachment	

TABLE II.- PHYSICAL PROPERTIES OF AID MATERIAL

Meridional tapes:

Width	1.27 cm (0.5 in.)
Breaking strength	2.22 kN (500 lbf)

Fabric:

Tensile strength (warp/fill)	16.8/14.4 kN/m (96/83 lbf/in.)
Tear strength	1.6/1.2 kN/m (9.0/6.8 lbf/in.)
Elongation, percent	28/29
Fabric density	63 g/m ² (1.86 ozm/yd ²)
Coating density	17 g/m ² (0.5 ozm/yd ²)
Thread count per inch	87/77
Permeability limit at 124 Pa (0.5 in. H ₂ O)	100 cm ³ /m ² -s (0.02 ft ³ /min/ft ²)

TABLE III.- MODEL DETAILS

Model	Aeroshell sting adapter	Burble fence	Inlet diameter				Nominal frontal area		Internal volume	
			Front		Rear		m ²	ft ²	m ³	ft ³
			cm	in.	cm	in.				
IA	Pivot	Yes	6.35	2.50	6.35	2.50	1.824	19.63	0.5456	17.89
IB	Pivot	Yes	6.35	2.50	4.60	1.81	1.824	19.63	.5456	17.89
IC	Rigid	Yes	6.35	2.50	6.35	2.50	1.824	19.63	.5456	17.89
IIA	Pivot	No	6.35	2.50	6.35	2.50	1.510	16.25	.4171	14.73
IIB	Rigid	No	6.35	2.50	6.35	2.50	1.510	16.25	.4171	14.73

TABLE IV.- AID TEST CONDITIONS

Model	Deployment conditions				Limits of test conditions				Total time in stream, min
	M	q		α , deg	M	q		α , deg	
		Pa	psf			Pa	psf		
IA	3.0	5750	120	0	3.0 to 4.5	2630 to 5750	55 to 120	0 to 10	48
IB	3.0	5750	120	0	2.4 to 3.0	5750	120	0 to 10	15
IC	3.0	5750	120	5	3.0	2590 to 5750	54 to 120	0 to 10	6
IIA	3.0	5750	120	0	3.0 to 3.7	1240 to 5750	26 to 120	0 to 10	30
IIB	3.0	5750	120	10	3.0 to 3.7	2630 to 5750	55 to 120	0 to 10	23

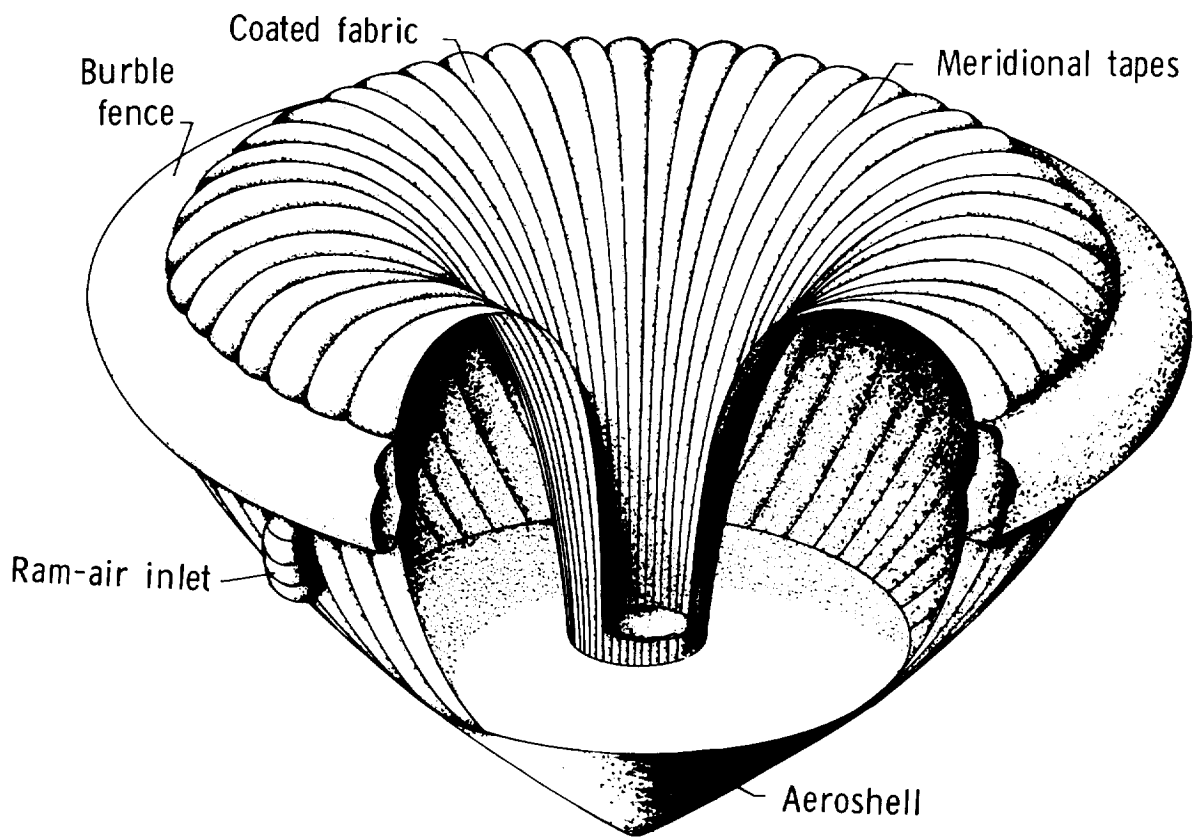
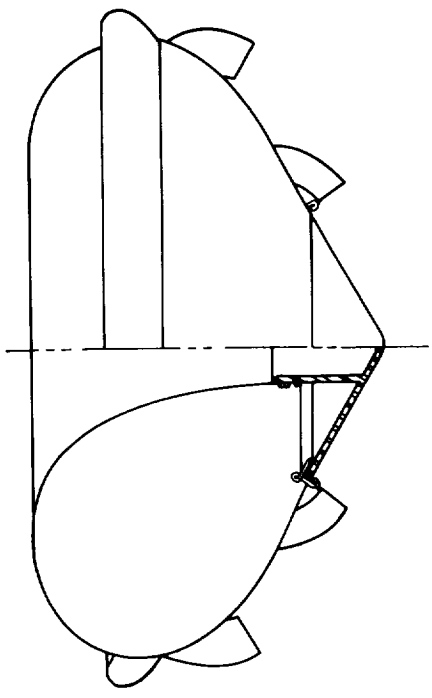
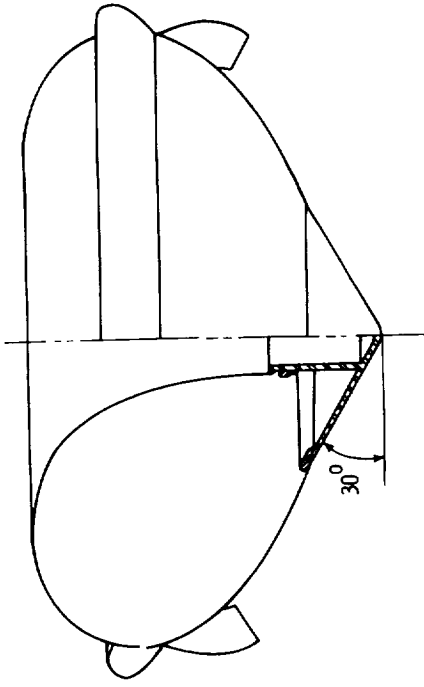


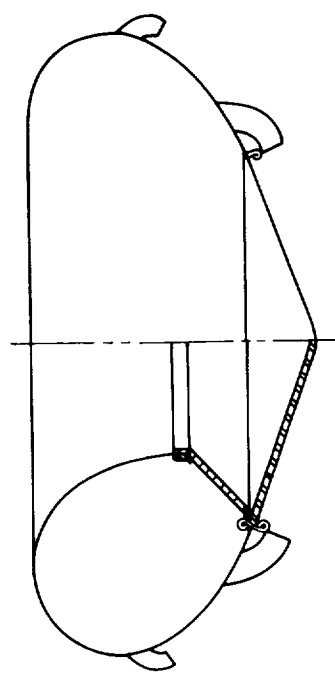
Figure 1.- Cutaway view of attached inflatable decelerator (AID).



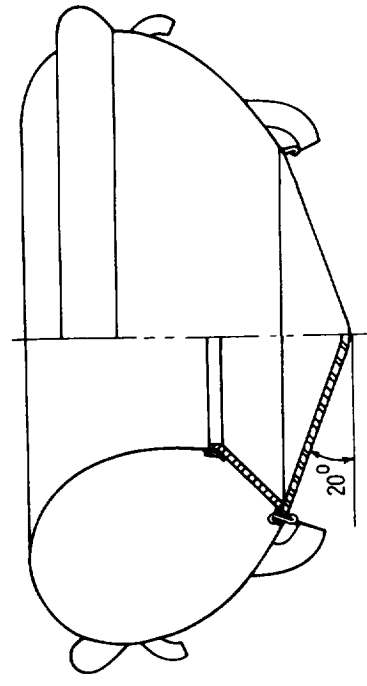
(b) AID with deployment by ram-air and C_{DA} ratio of 4.5 (ref. 11).



(a) AID with deployment initiated by water vaporization and C_{DA} ratio of 4.5 (ref. 8).

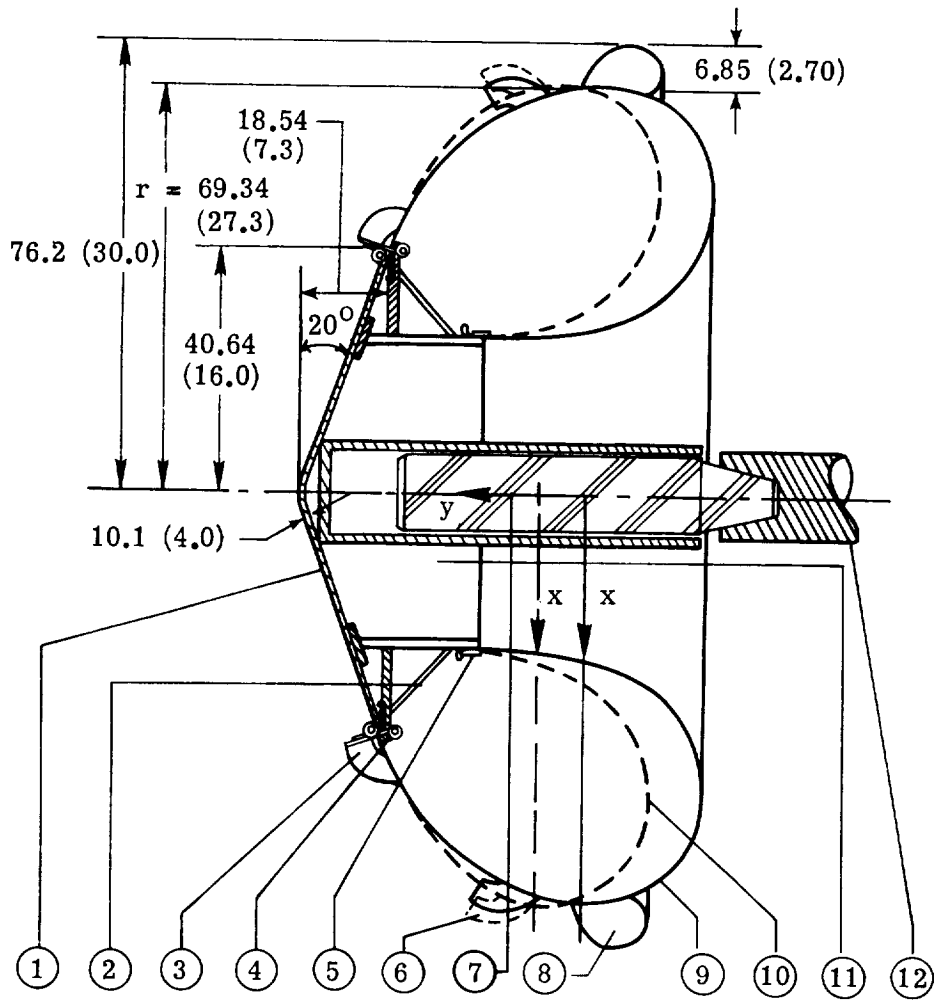


(d) AID with C_{DA} ratio of 2.5 without burble fence, present investigation.



(c) AID with C_{DA} ratio of 2.5, present investigation.

Figure 2.- Progression of AID development.



1. Aeroshell
2. Decelerator stowage compartment
3. Forward inlets, rotated 45° (typ. 4 places)
4. Decelerator clamp (outer)
5. Decelerator clamp (inner)
6. Aft inlets (typ. 4 places)
7. Six-component balance
8. Burble fence
9. Inflatable decelerator, with burble fence
10. Inflatable decelerator, without burble fence
11. Payload stowage compartment
12. Sting support

Figure 3.- Details of AID models. All dimensions are in centimeters (in.).

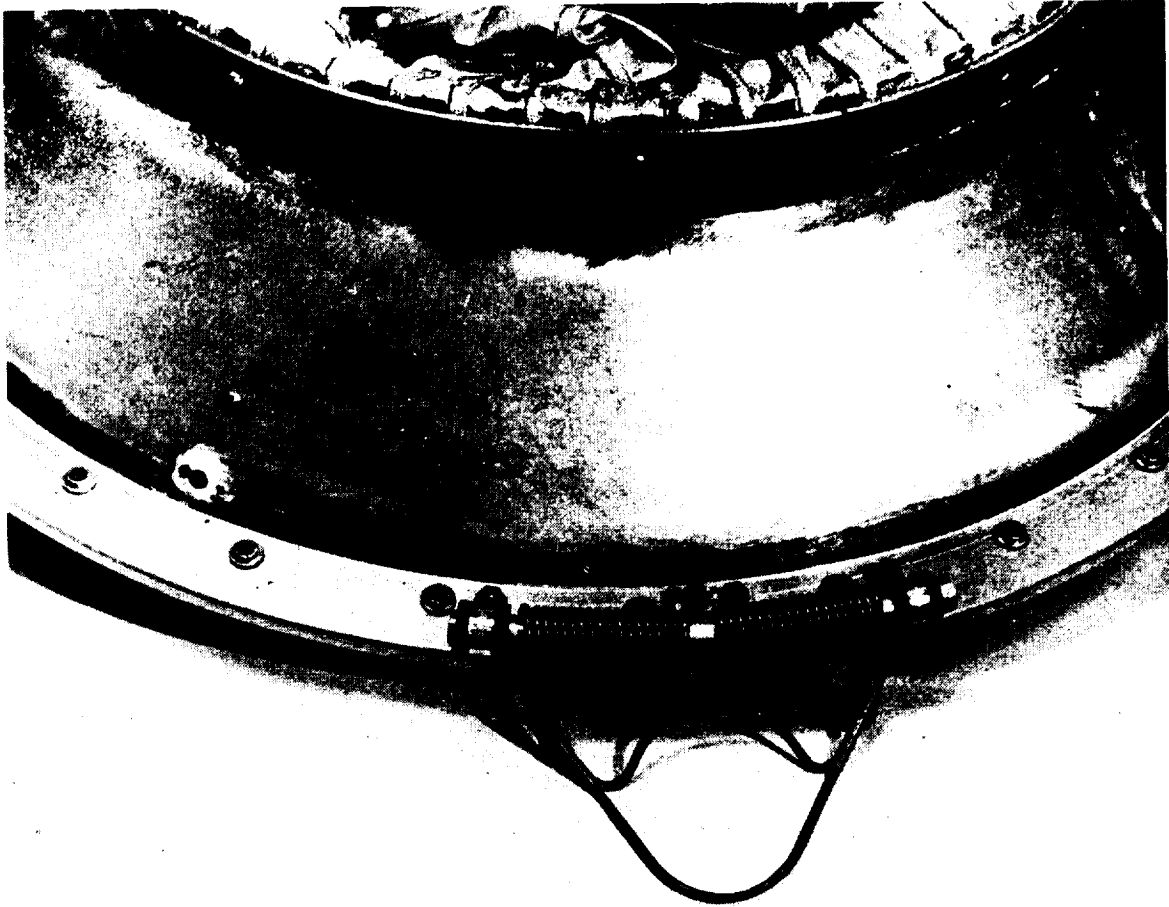


Figure 4.- Forward inlet spring attached to hard structure. L-74 1061

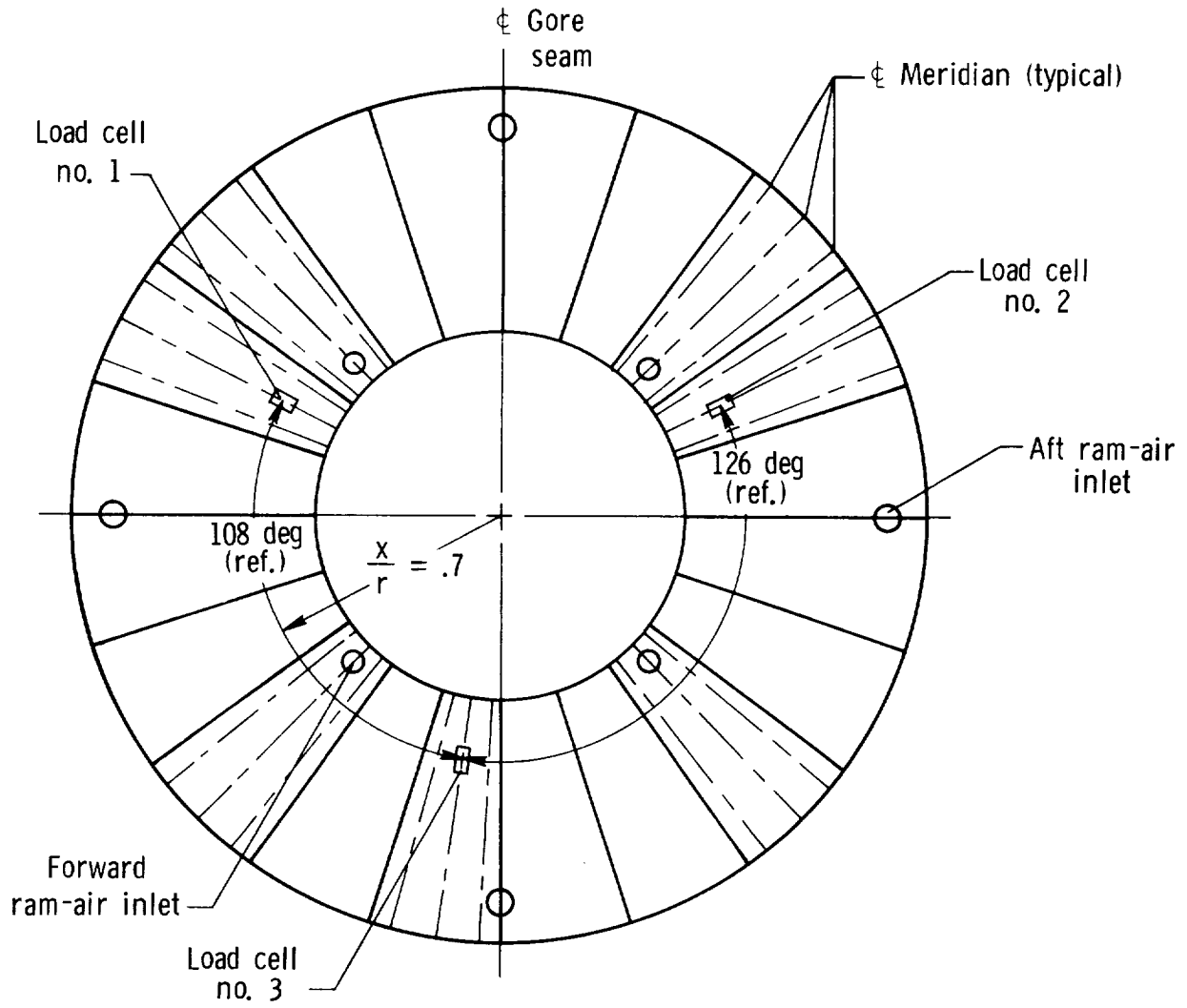


Figure 5.- Meridian-tape load-cell locations (looking downstream).

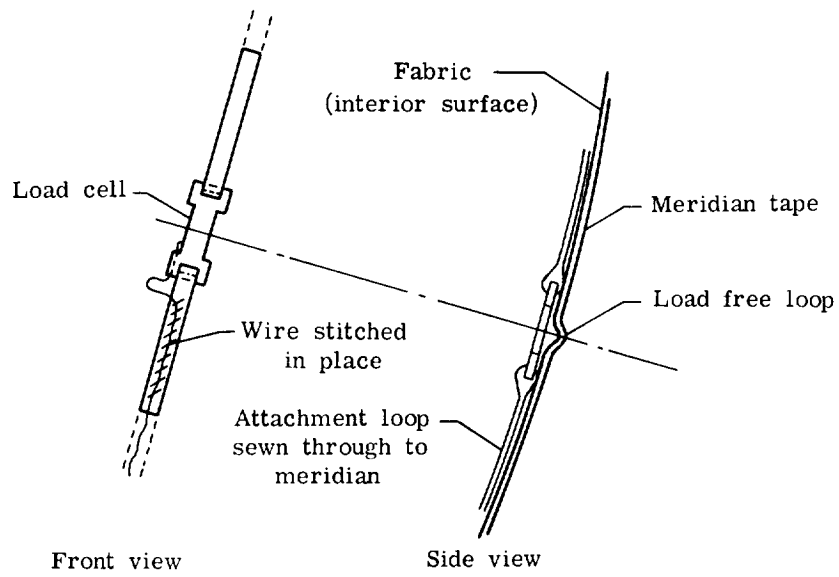


Figure 6.- Load cell attachment to meridian.

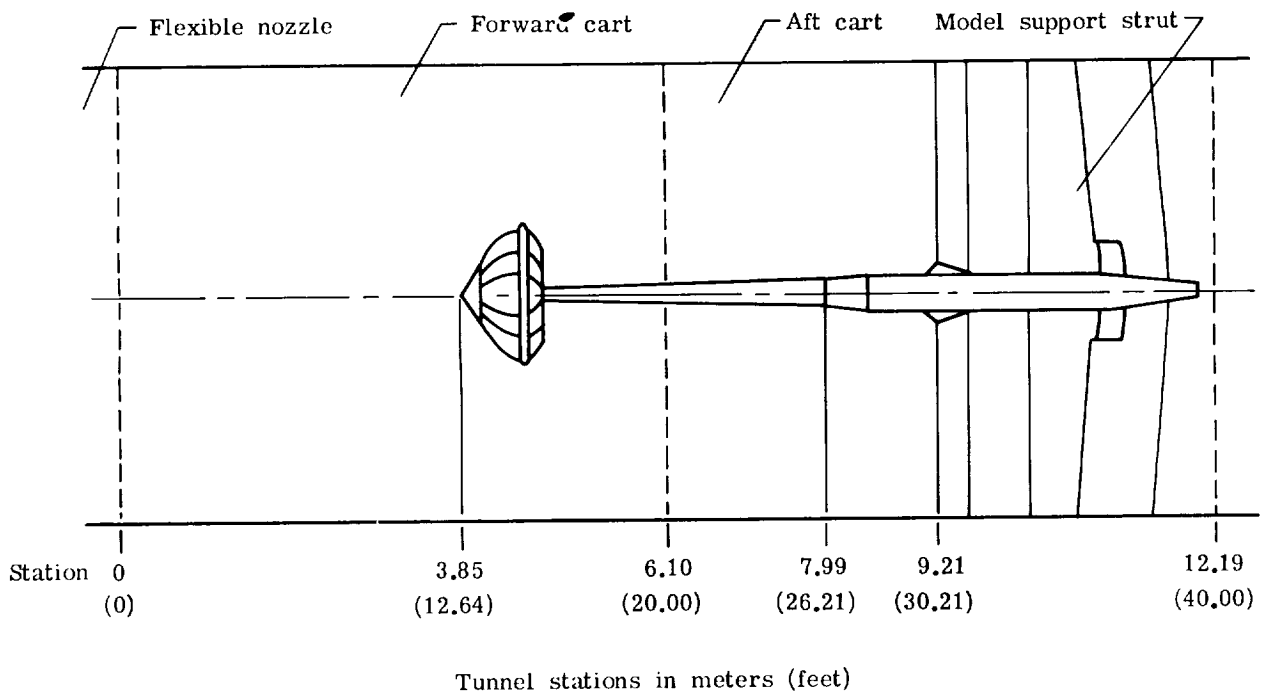


Figure 7.- Location of model in test section.

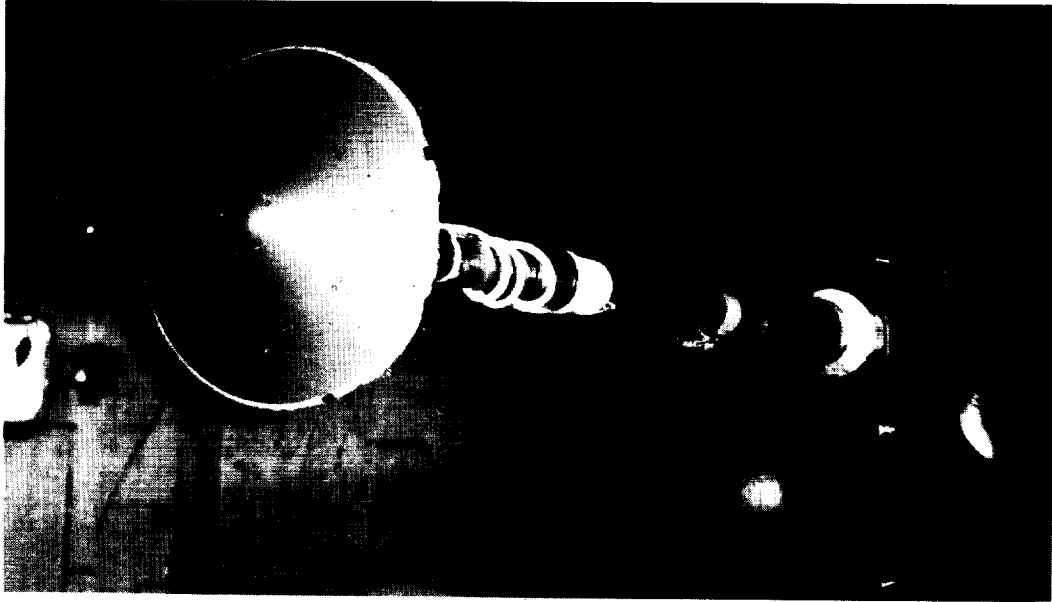


Figure 8.- Model mounted on sting in AEDC 16-ft propulsion wind tunnel (16S). L-74-1062

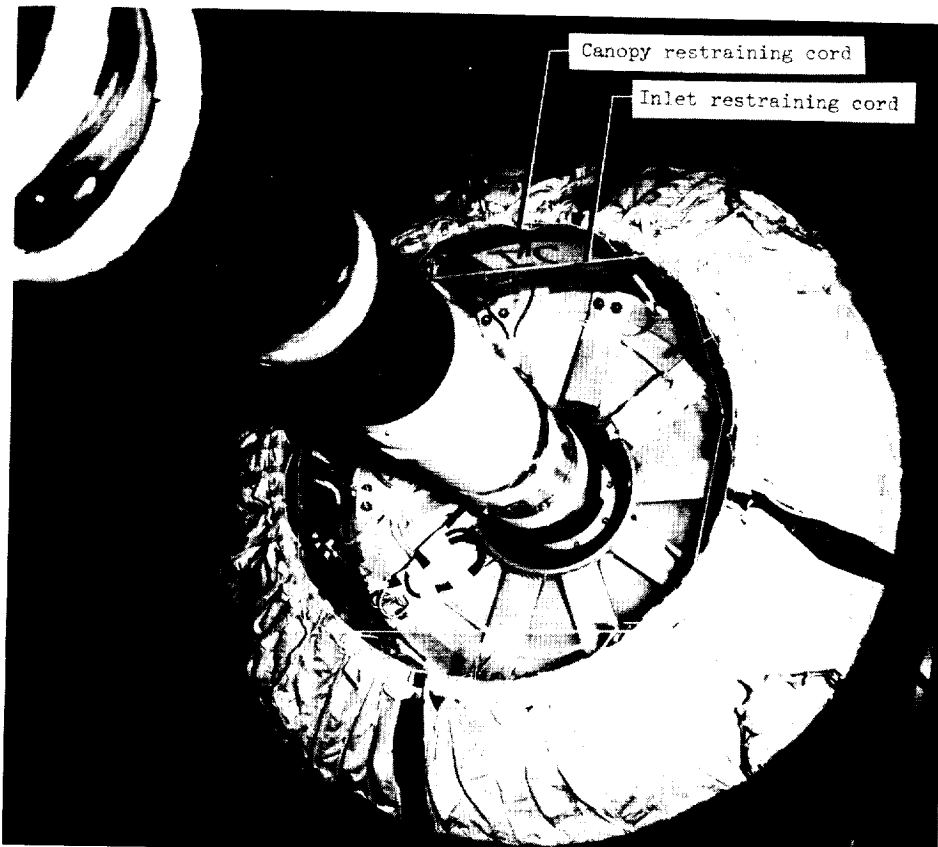
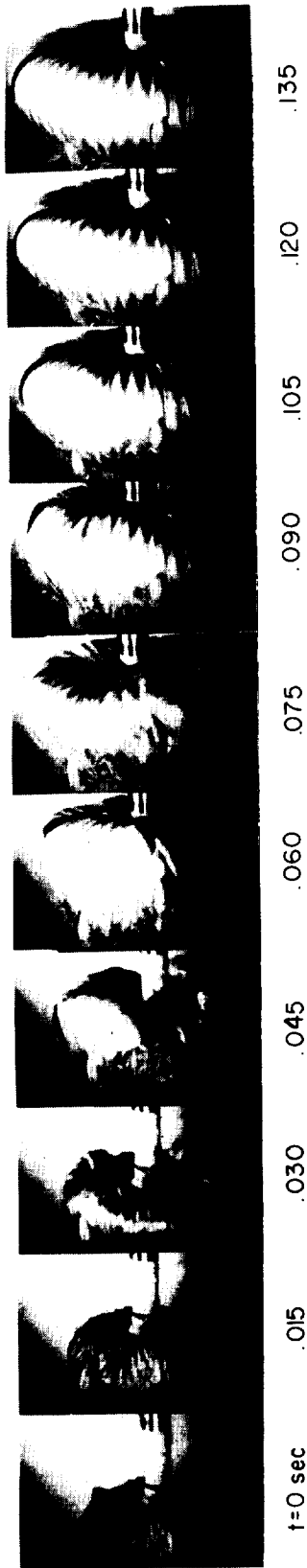
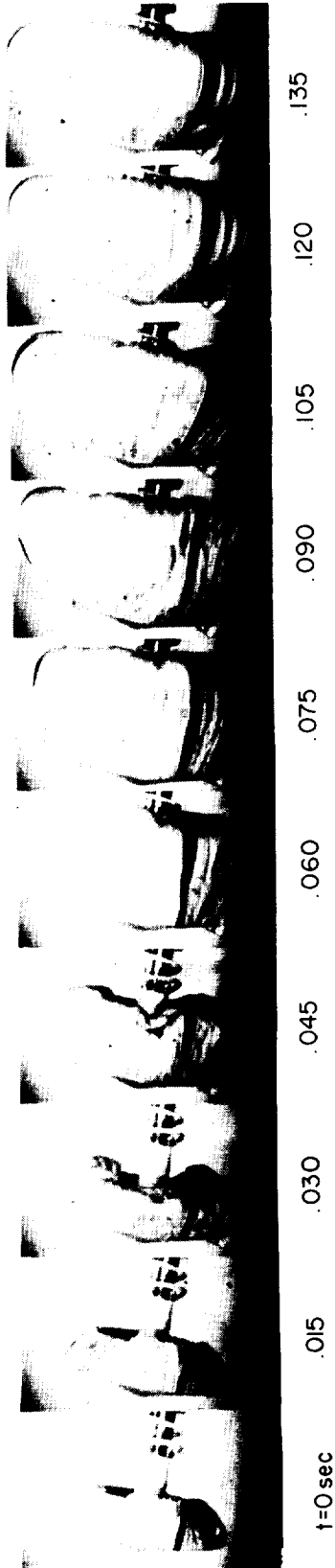


Figure 9.- Packaged AID on sting in AEDC 16-ft propulsion wind tunnel (16S). L-74-1063



(a) Model IIA; $\alpha = 0^\circ$.



(b) Model IIB; $\alpha = 10^\circ$.

Figure 10.- Photographs of the deployment sequence, side view.

L-74-1064

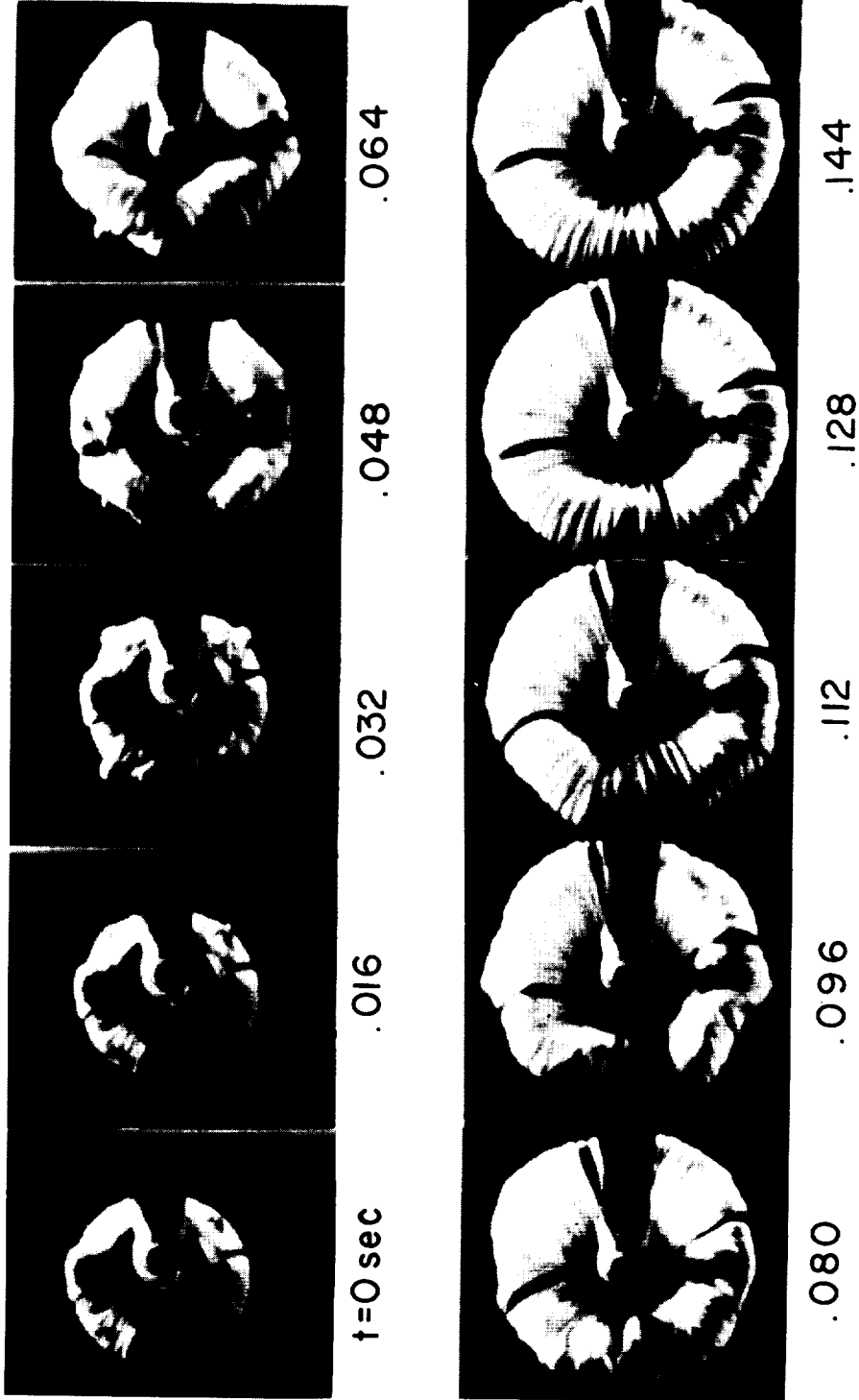
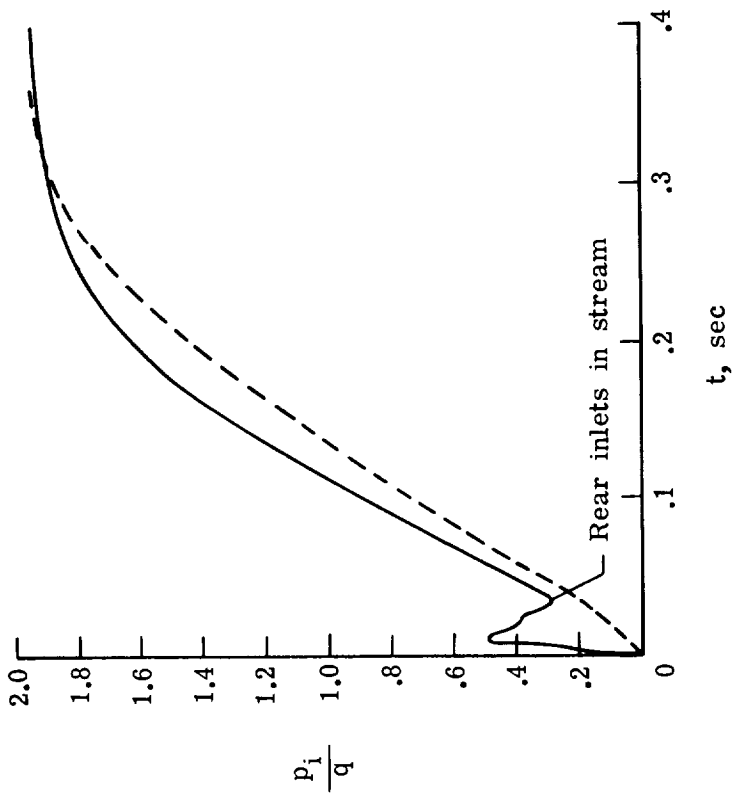
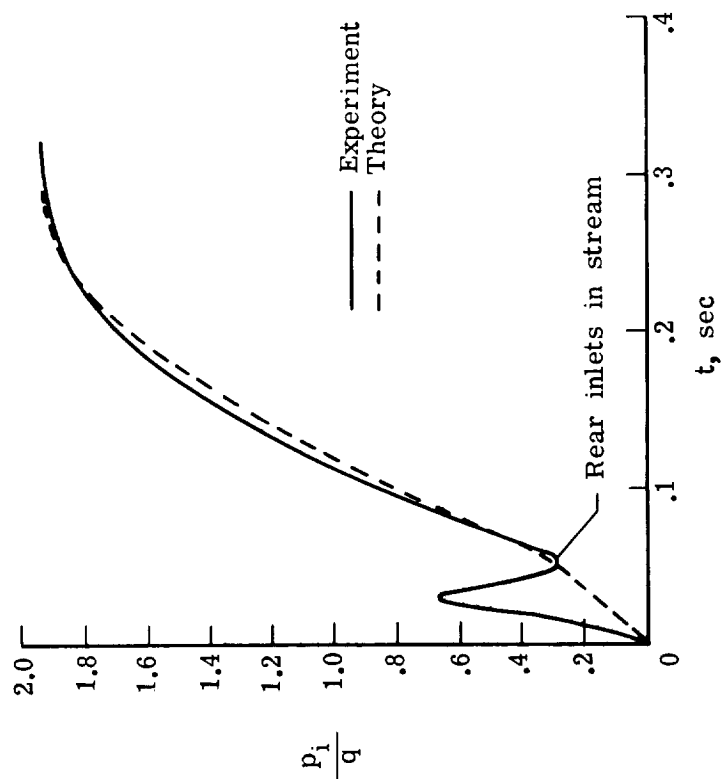


Figure 11.- Rear view of the deployment sequence of model IIB.

L-74-1065



(a) Model IA.



(b) Model IA.

Figure 12.- Inflation history measured during AID deployment. $M = 3.0$; $q = 5750$ Pa (120 psf).

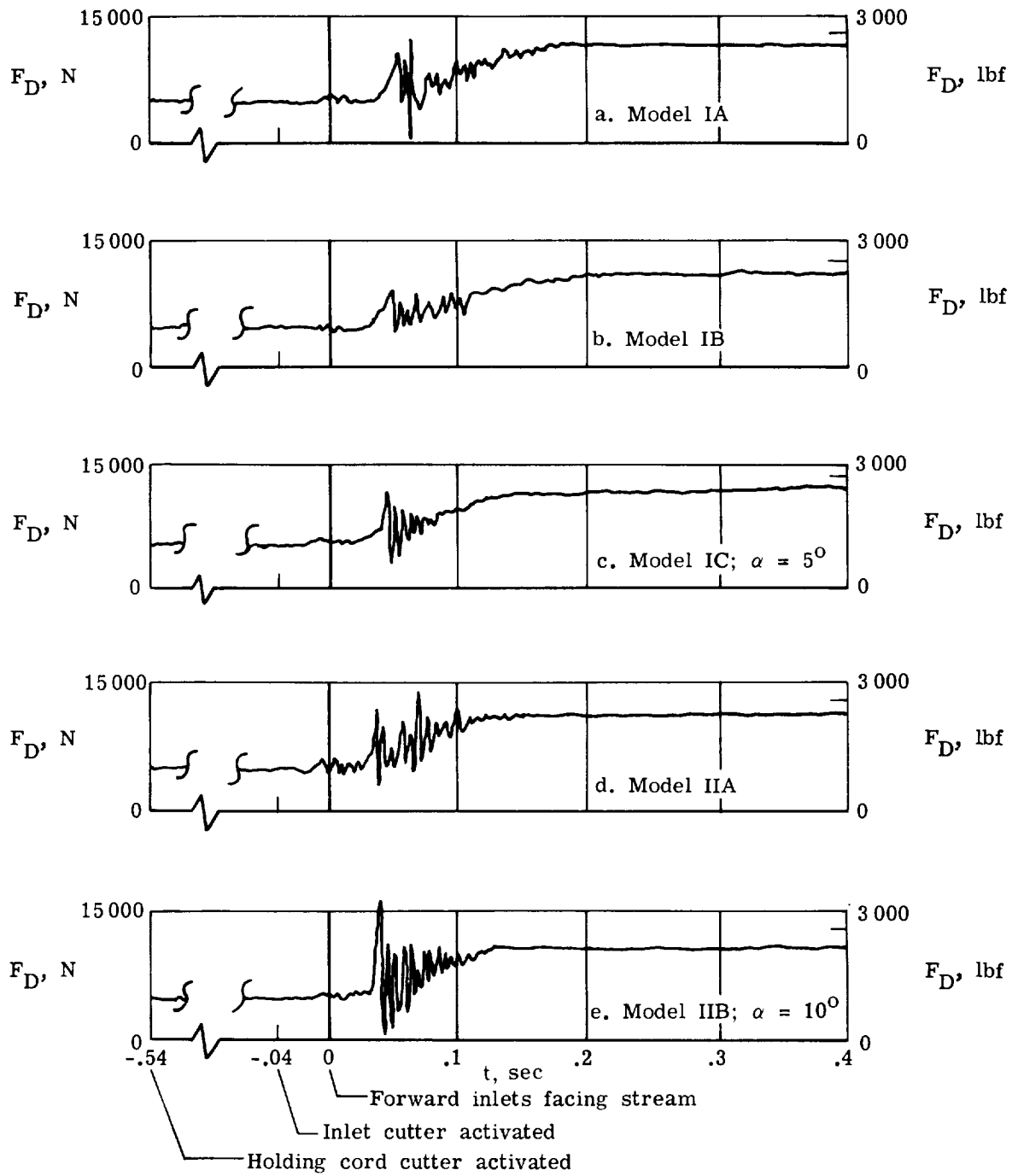
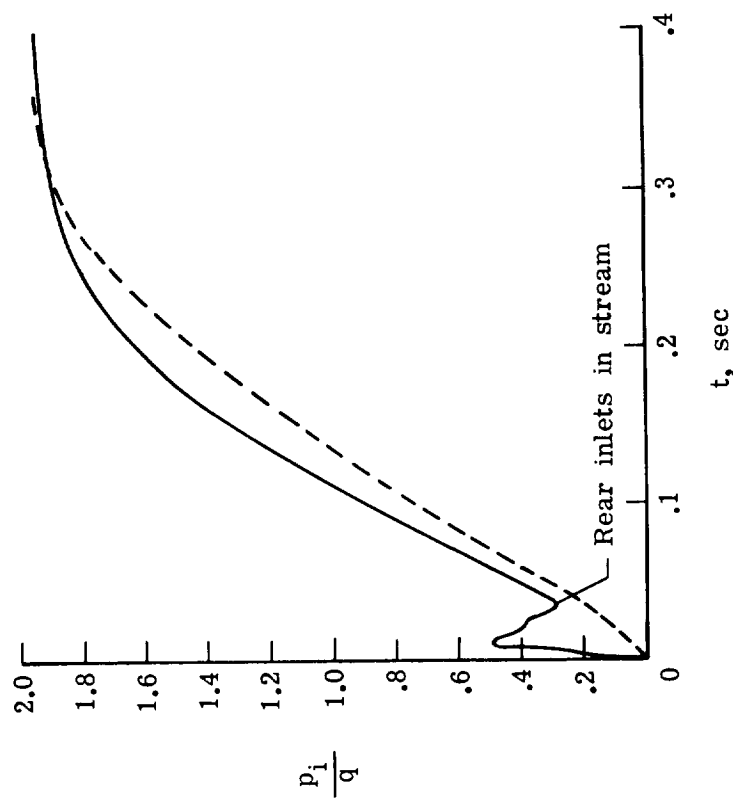
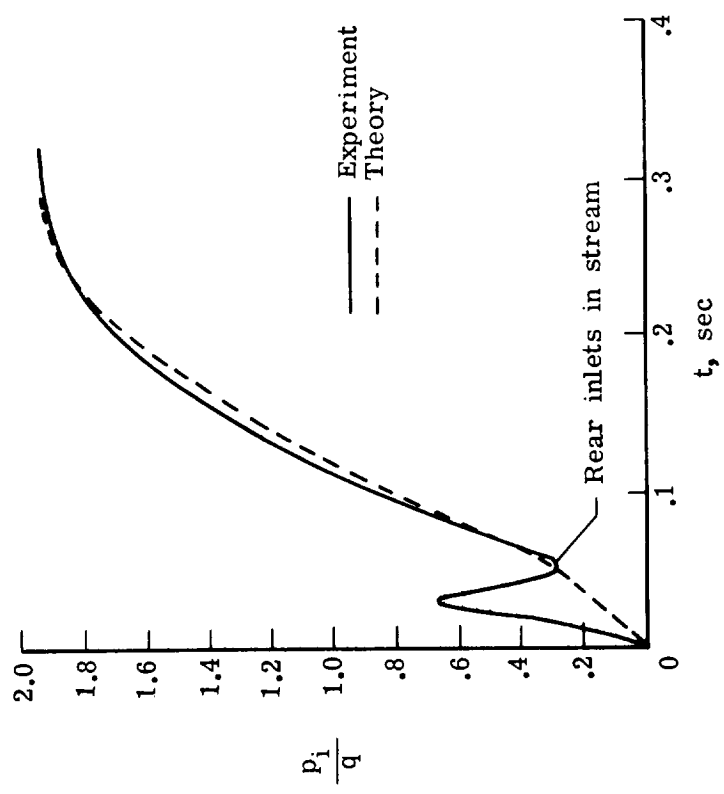


Figure 13.- Axial force during AID deployment. $M = 3.0$; $q = 5750 \text{ Pa}$ (120 psf).



(a) Model IA.



(b) Model IA.

Figure 12. - Inflation history measured during AID deployment. $M = 3.0$; $q = 5750$ Pa (120 psf).

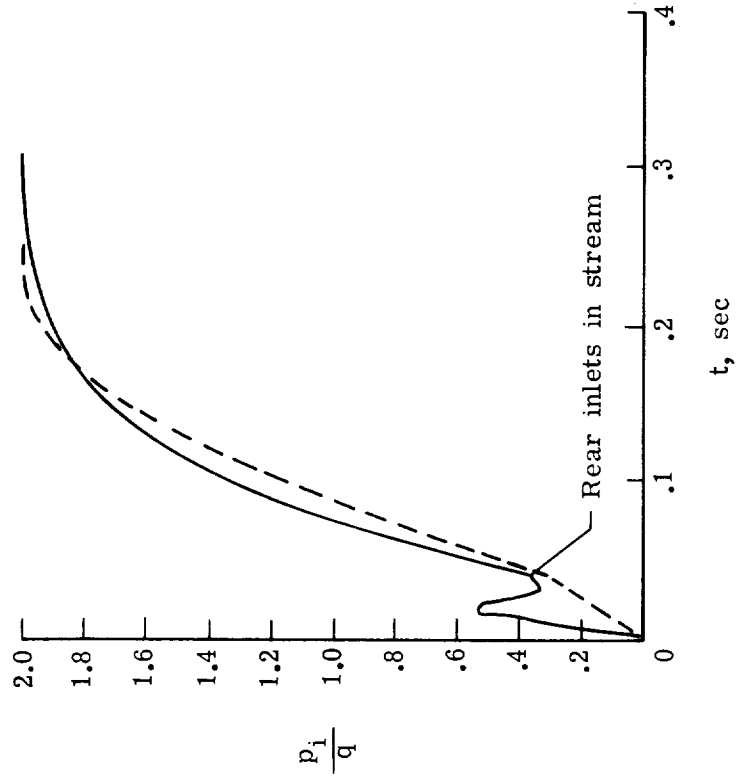
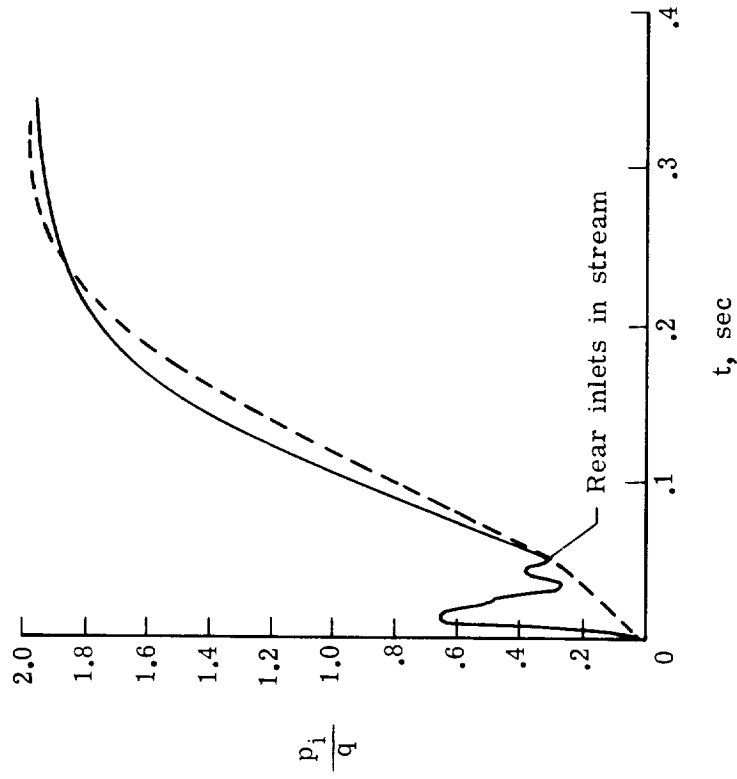
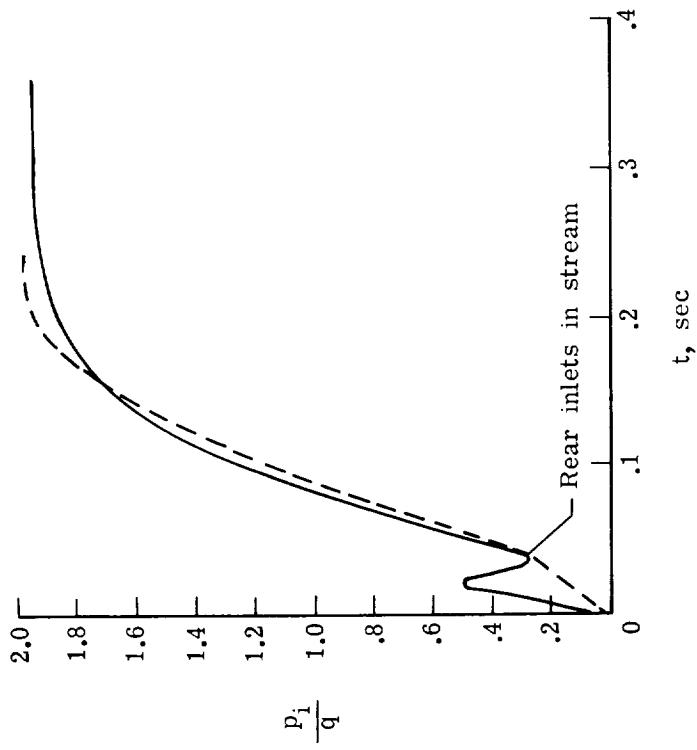


Figure 12.- Continued.



(e) Model IIB; $\alpha = 10^\circ$.

Figure 12.- Concluded.

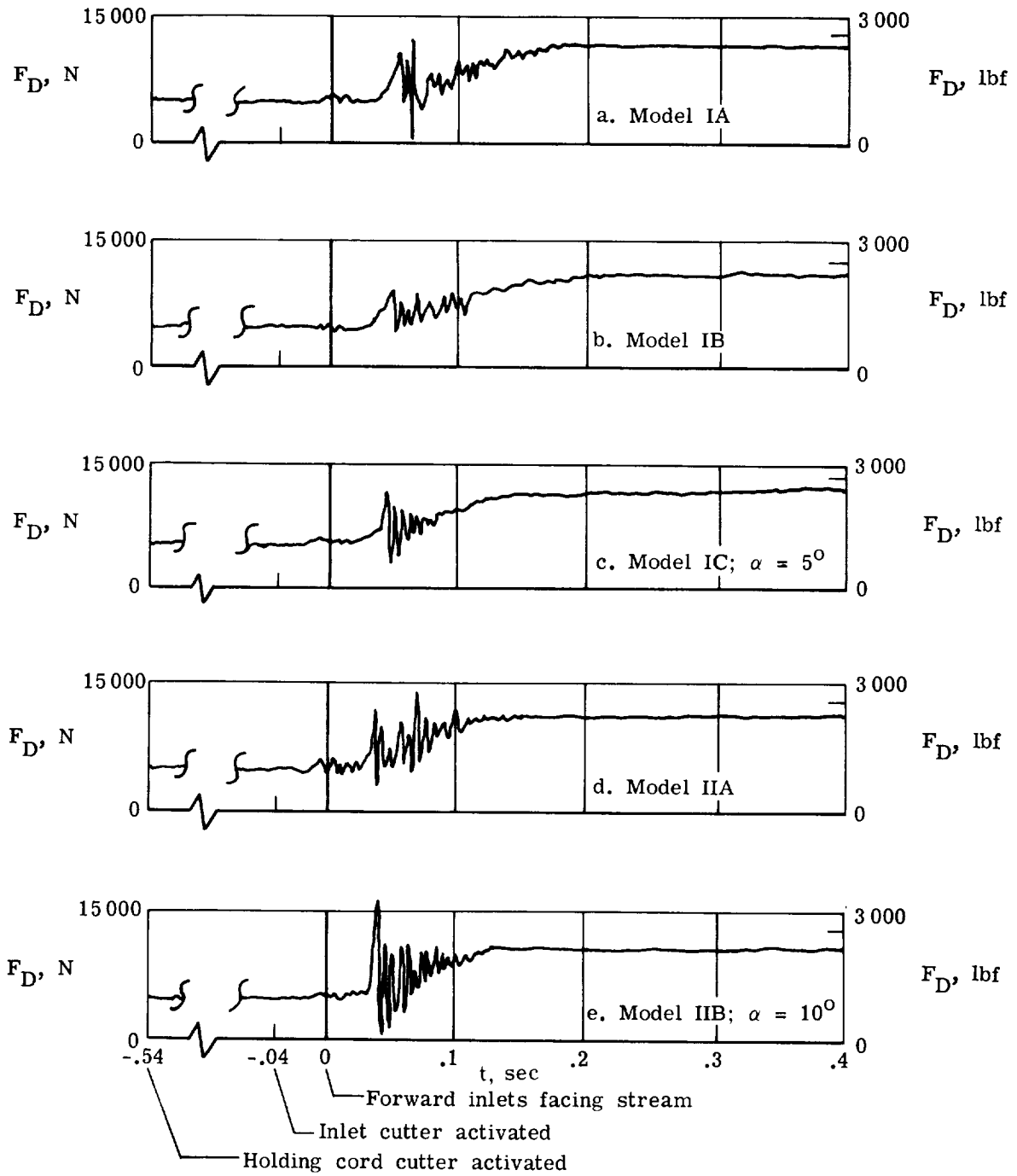
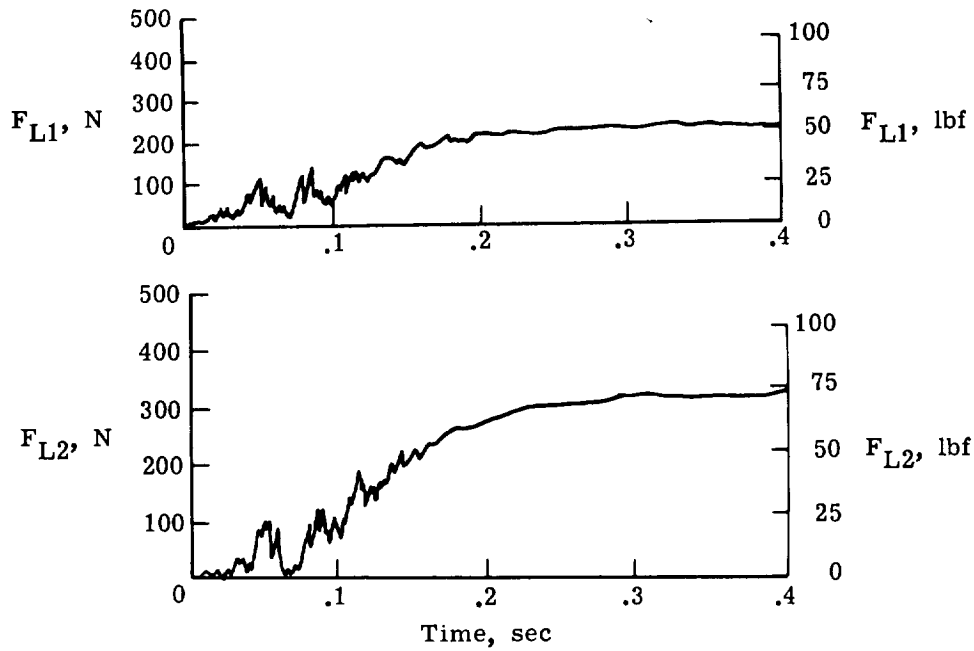
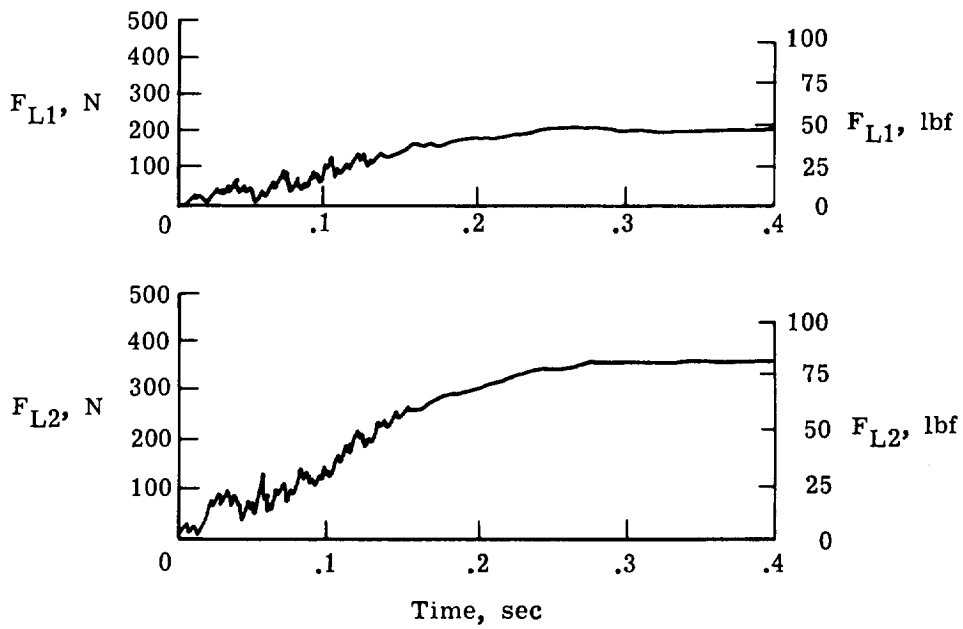


Figure 13.- Axial force during AID deployment. $M = 3.0$; $q = 5750$ Pa (120 psf).

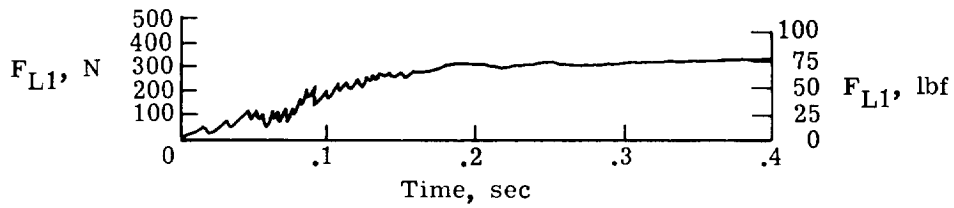


(a) Model IA.

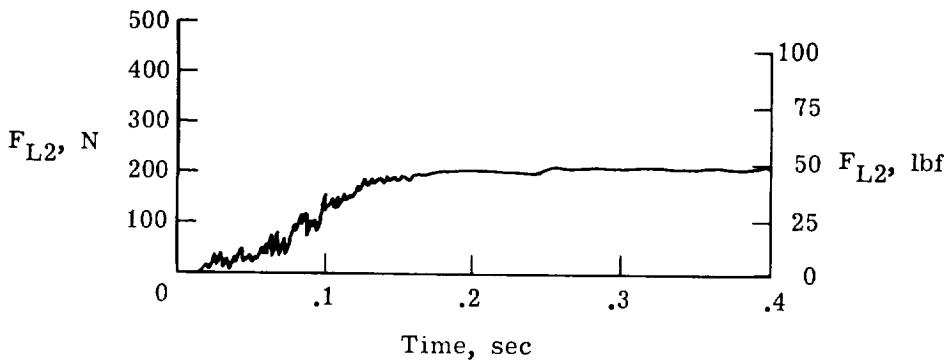
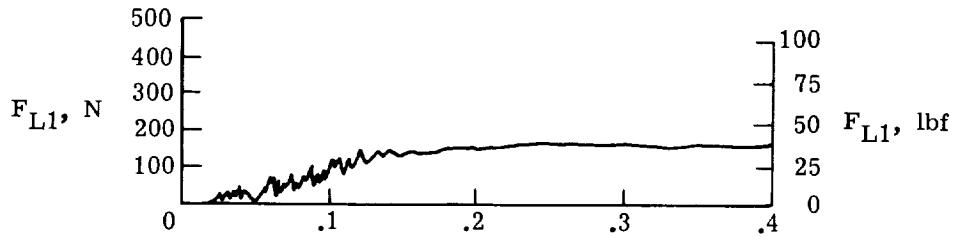


(b) Model IB.

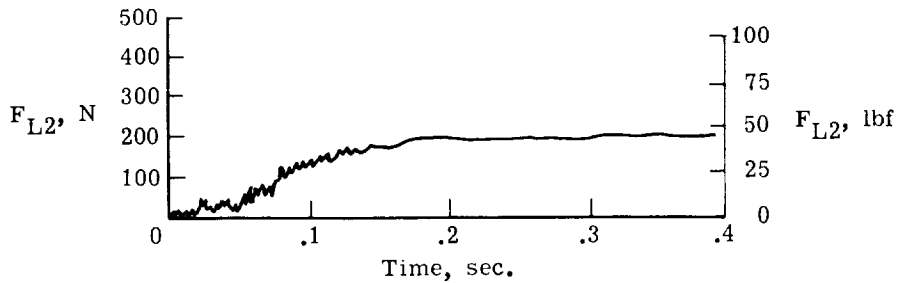
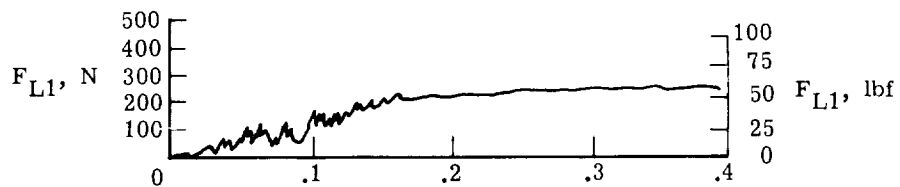
Figure 14.- Meridian-tape response from load cells 1 and 2 during deployment.
 $M = 3.0$; $q = 5750 \text{ Pa}$ (120 psi).



(c) Model IC; $\alpha = 5^\circ$.

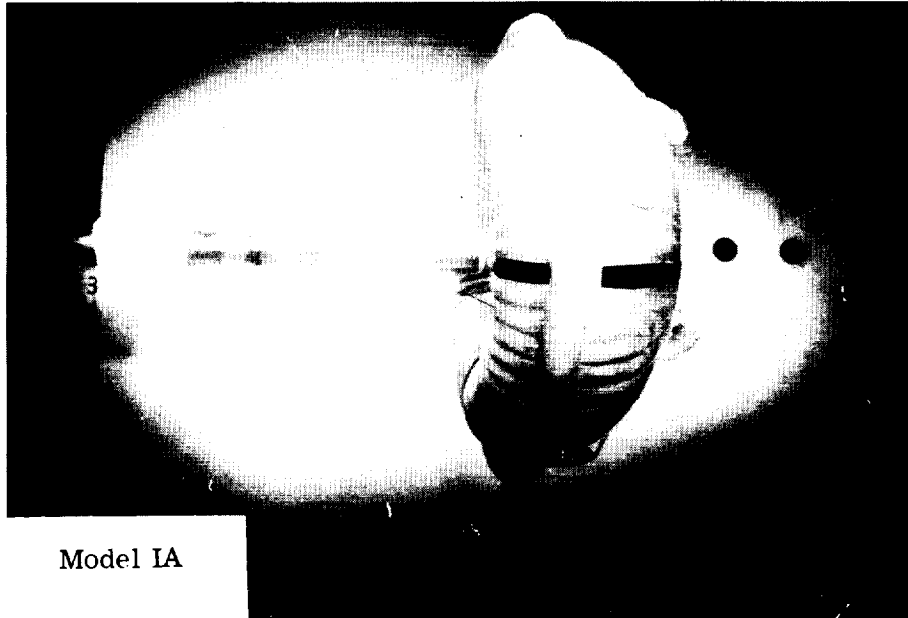


(d) Model IIA.

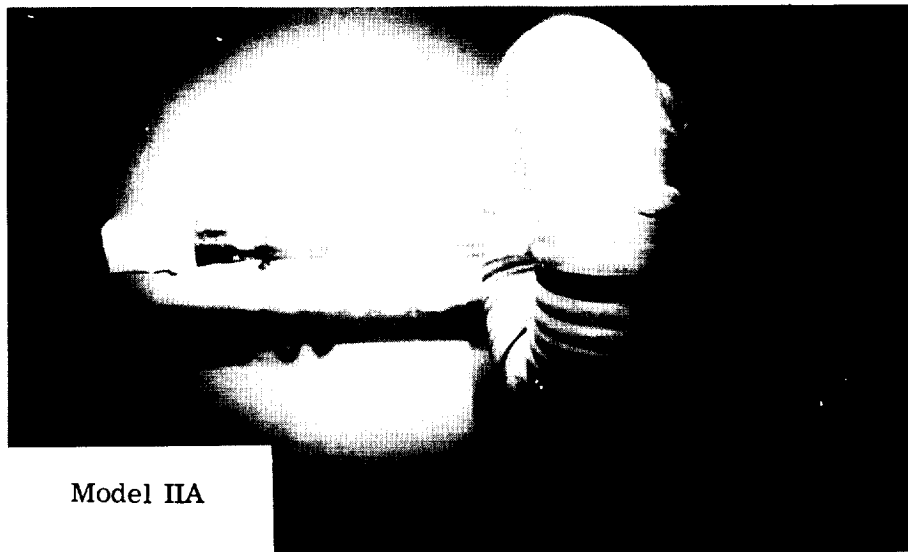


(e) Model IIB; $\alpha = 10^\circ$.

Figure 14.- Concluded.



Model IA



Model IIA

L-74-1066

Figure 15.- Deployed AID in Mach 3 stream.

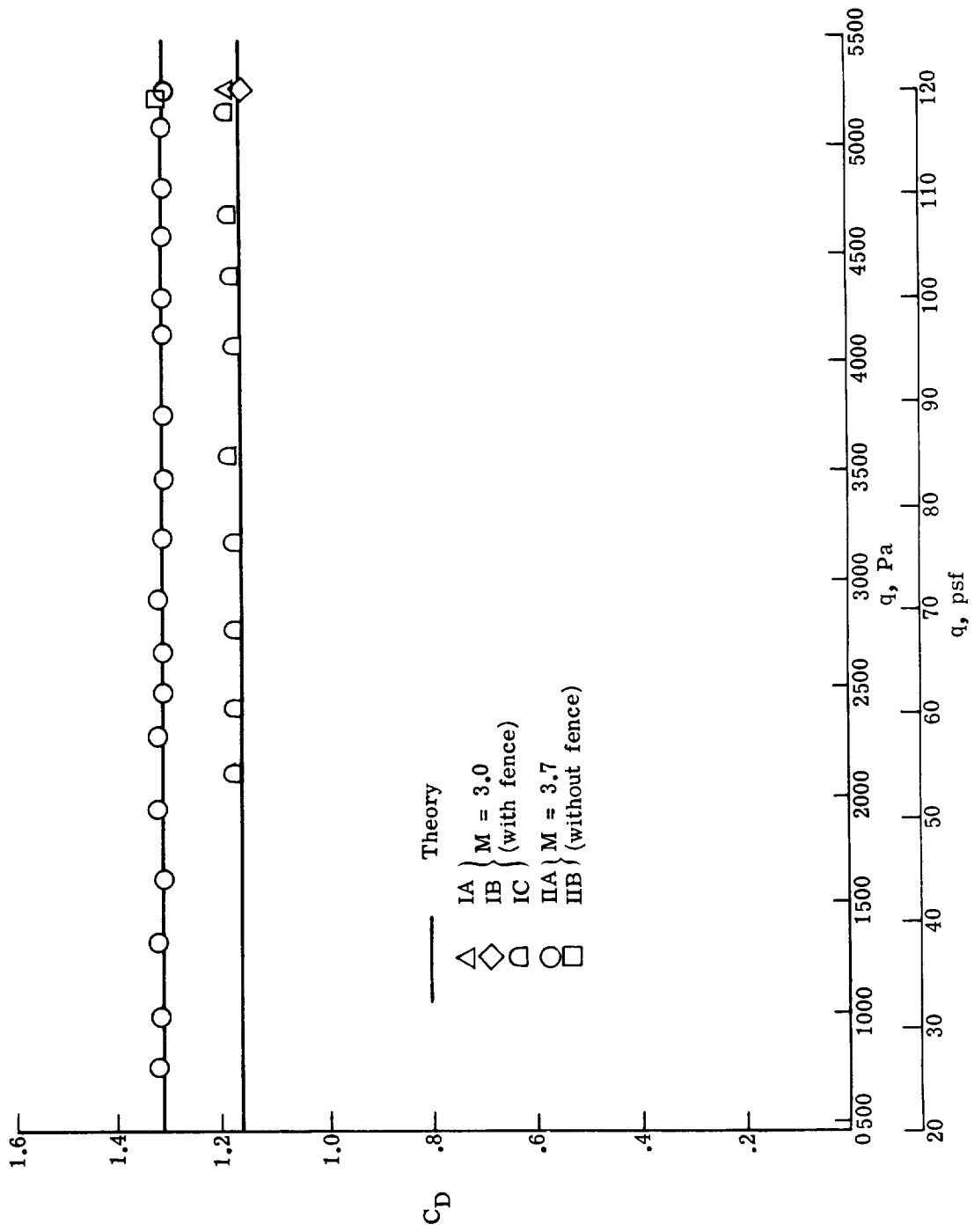


Figure 16.- Influence of dynamic pressure on drag coefficient.

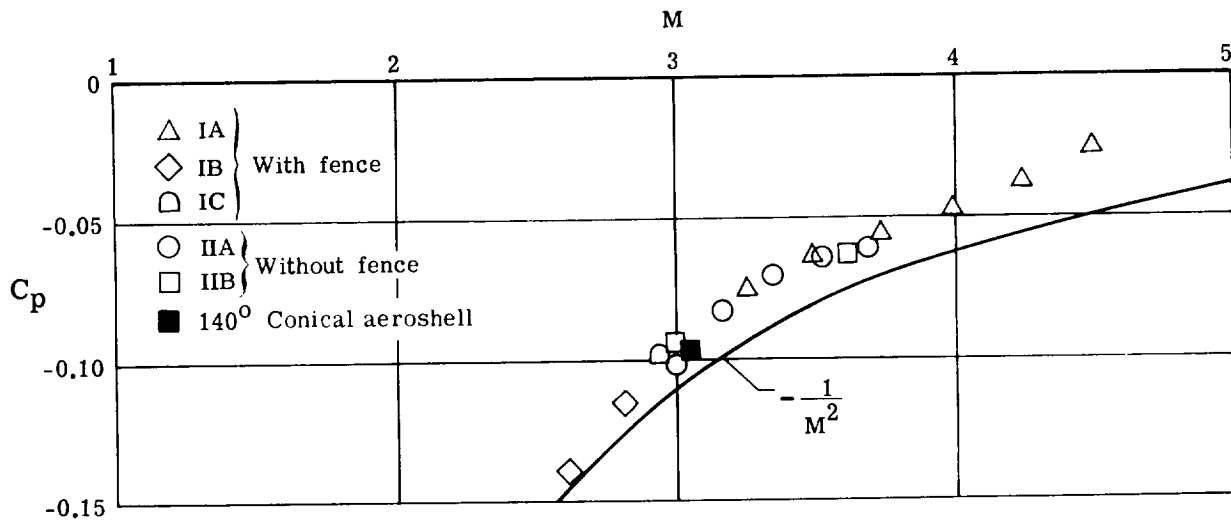


Figure 17.- Effects of Mach number on base pressure coefficient of AID.

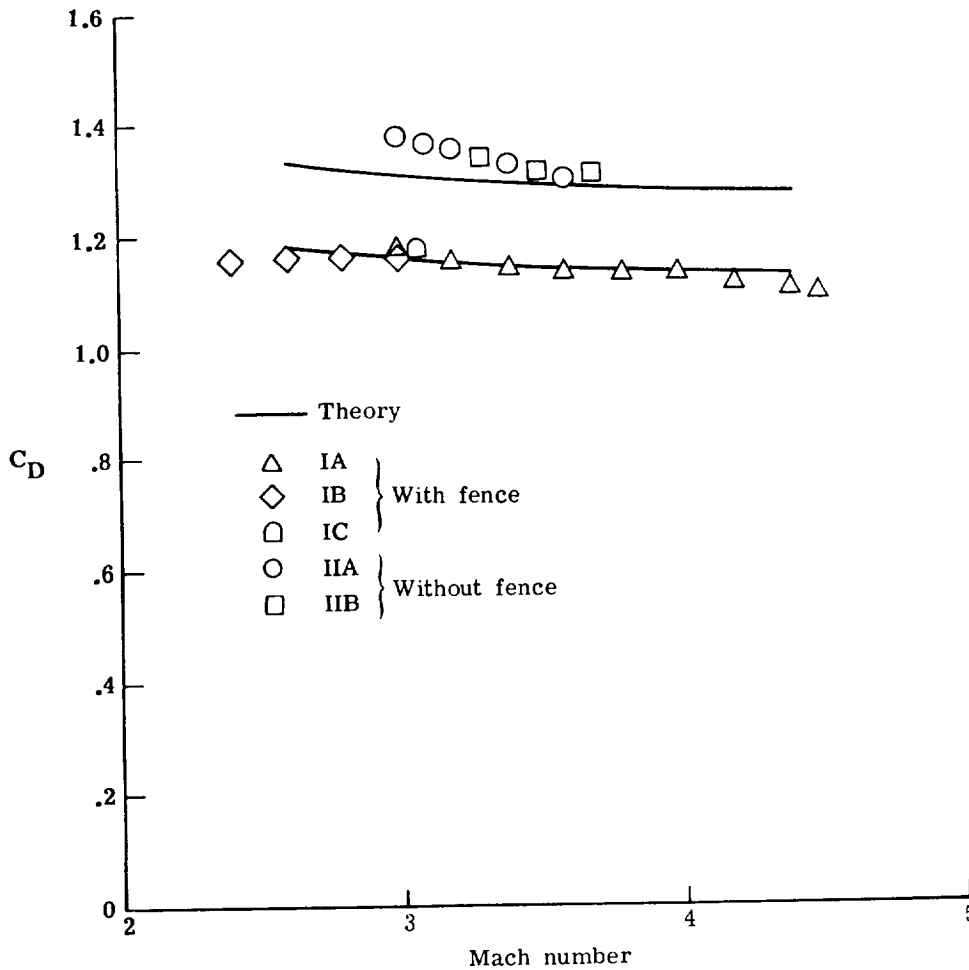


Figure 18.- Influence of Mach number on drag coefficient.

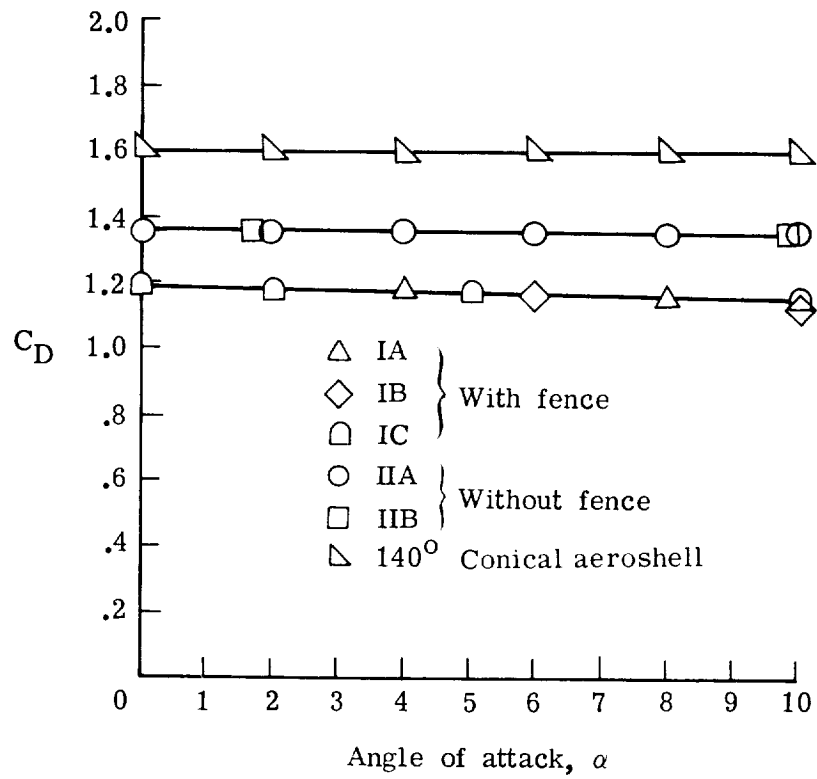


Figure 19.- Effects of angle of attack on drag coefficient.

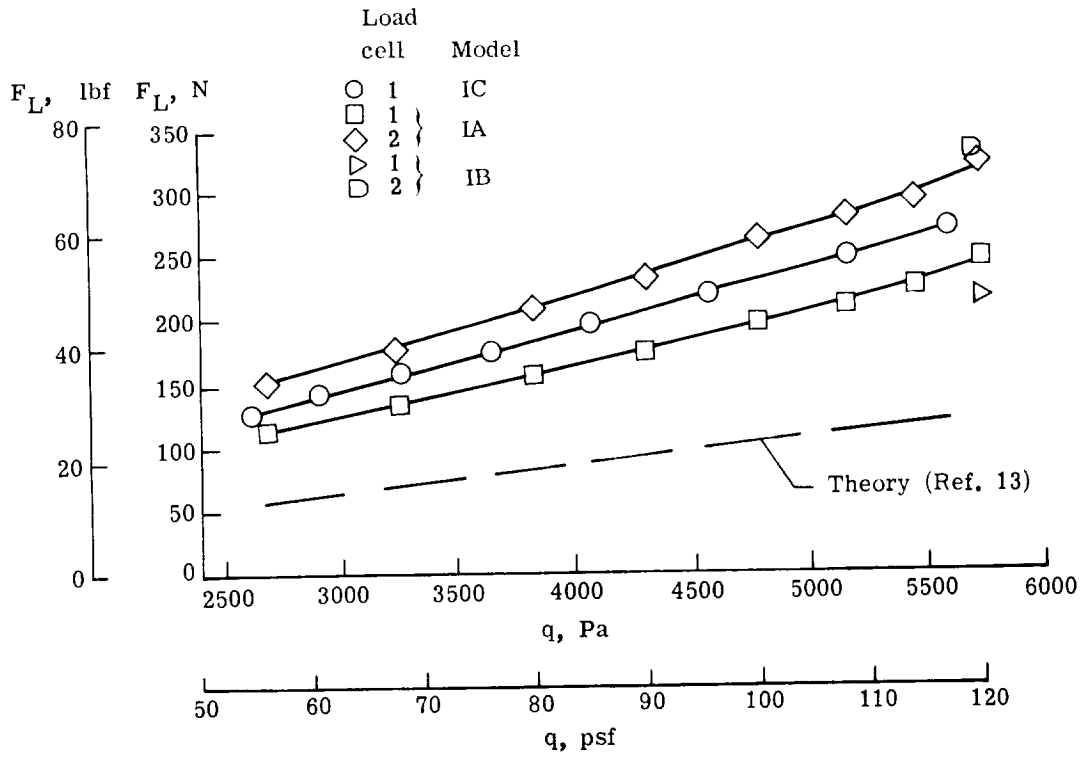


Figure 20.- Measured and calculated forces in meridian tapes for model I.

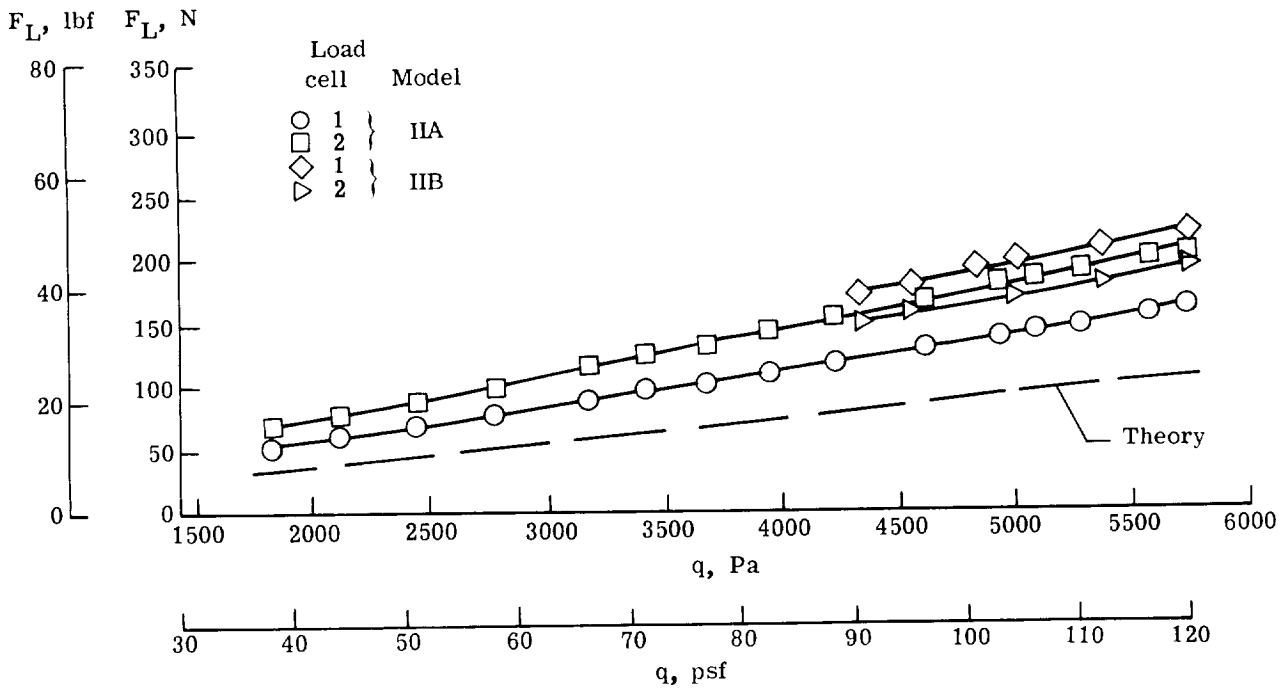


Figure 21.- Measured and calculated forces in meridian tapes for model II.

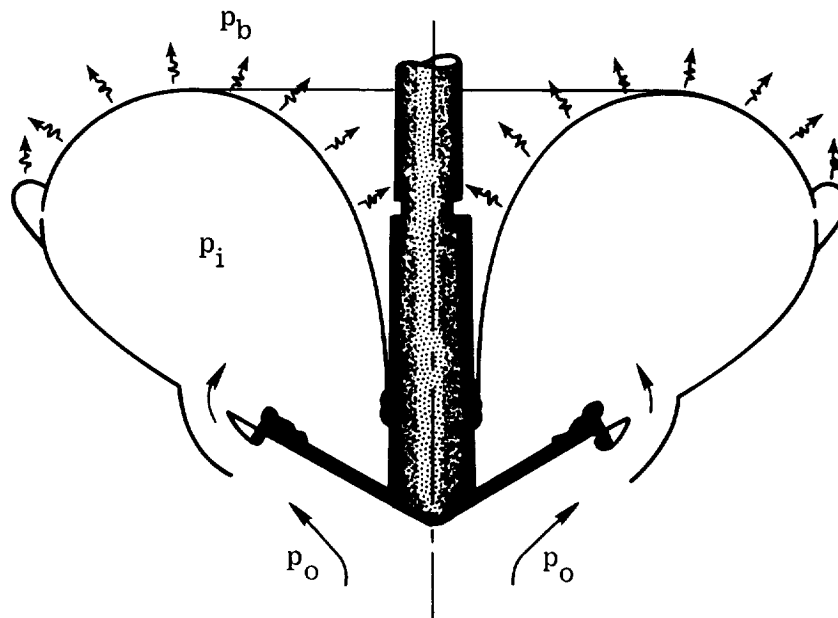


Figure 22.- Flow model for ram-air inflation analysis.